Biomaterials 30 (2009) 1746–1755

Contents lists available at ScienceDirect

Biomaterials

journal homepage: www.elsevier.com/locate/biomaterials

Delivery of sodium borocaptate to glioma cells using immunoliposome conjugated with anti-EGFR antibodies by ZZ-His

Bin Feng [a], Kazuhito Tomizawa [a,b,*], Hiroyuki Michiue [a], Shin-ichi Miyatake [c], Xiao-Jian Han [a], Atsushi Fujimura [a], Masaharu Seno [e], Mitsunori Kirihata [d], Hideki Matsui [a]

[a] Department of Physiology, Okayama University Graduate School of Medicine, Dentistry and Pharmaceutical Sciences, 2-5-1 Shikata-cho, Okayama 700-8558, Japan
[b] Department of Molecular Physiology, Faculty of Medical and Pharmaceutical Sciences, Kumamoto University, Kumamoto 860-8558, Japan
[c] Department of Neurosurgery, Osaka Medical College, 2-7 Daigaku-machi, Takatsuki Osaka 569-8686, Japan
[d] Department of Bioscience and Informatics, Graduate School of Life and Environmental Sciences, Osaka Prefecture University, 1-1 Gakuen-machi, Sakai 599-8531, Japan
[e] Department of Bioscience and Biotechnology, Faculty of Engineering, Okayama University Graduate School of Natural Science and Technology, Okayama 700-8530, Japan

ARTICLE INFO

Article history:
Received 1 October 2008
Accepted 4 December 2008
Available online 1 January 2009

Keywords:
Glioma cells
BNCT
EGFR
Immunoliposome
Drug delivery

ABSTRACT

Nanoparticles are effective of delivering cargo into cells. Here, sodium borocaptate (BSH) was encapsulated in liposomes composed of nickel lipid, and anti-epidermal growth factor receptor (EGFR) antibodies were conjugated to the liposomes using the antibody affinity motif of protein A (ZZ) as an adaptor (immunoliposomes). The immunoliposomes were used to deliver BSH into EGFR-overexpressing glioma cells. Immunohistochemical analysis using an anti-BSH monoclonal antibody revealed that BSH was delivered effectively into the cells but not into EGFR-deficient glioma or primary astrocytes. In an animal model of brain tumors, both the liposomes and the BSH were only observed in the tumor. Moreover, the efficiency of ^{10}B's delivery into glioma cells was confirmed by inductively coupled plasma-atomic emission spectrometry (ICP-AES) both *in vitro* and *in vivo*. The results suggest that this system utilizing immunoliposomes provides an effective means of delivering ^{10}B into glioma cells in boron neutron capture therapy (BNCT).

1. Introduction

Glioblastoma multiforme (GBM) is one of the most malignant and aggressive brain tumors. Although at present, treatment mainly consists of surgery and radiotherapy [1], it is difficult to remove all tumor tissues without severe damage to the brain, and healthy brain tissue is less tolerant of conventional radiotherapy than tumor tissue.

Boron neutron capture therapy (BNCT) provides a way to selectively destroy malignant cells and spare normal cells. BNCT is a binary method for the treatment of cancer based on the tumor-selective delivery of ^{10}B followed by radiation with low energy thermal neutrons [2]. It is assumed that the selective accumulation of ^{10}B in tumors will cause the killing of cancer cells and induce a therapeutic effect [3]. BNCT has been applied clinically for the treatment of malignant brain tumors, malignant melanoma, head and neck cancer, and hepatoma [4]. For effective BNCT, enough ^{10}B must be encapsulated in the tumor and a high ratio of tumor to blood is needed. Different approaches have been proposed for delivering ^{10}B into tumor cells, including the use of boronated macromolecules such as monoclonal antibodies and microparticles such as liposomes, etc. [2]. However, these methods have several disadvantages, such as low delivery efficiency, a lack of specificity and stability *in vivo*, and the high cost of preparing nanoparticles. Two boron compounds, sodium borocaptate (BSH) and boronophenylalanine (BPA), are undergoing clinical trials [5]. BPA is an analog of an essential amino acid and actively carried to brain tumors. However, it also accumulates in normal brain tissue. By contrast, BSH accumulates little in normal tissue but accumulates insufficiently in tumors compared with BPA [6]. Therefore, an easy-to-prepare and universal ^{10}B delivery system is still awaited.

In recent years, drug delivery research has increasingly focused on antibody-targeting liposomes in the treatment of cancers including glioblastoma [7]. Liposomes are unilamellar phospholipid vesicles with high interior encapsulation for water-soluble compounds such as borane ions [8]. Targeted liposomes provide an advantage over untargeted liposomes not because of increased localization to tumor sites but because of increased interaction with

* Corresponding author. Department of Molecular Physiology, Faculty of Medical and Pharmaceutical Sciences, Kumamoto University, Kumamoto 860-8558, Japan. Tel.: +81 96 373 5050; fax: +81 96 373 5052.
E-mail address: tomikt@kumamoto-u.ac.jp (K. Tomizawa).

0142-9612/$ – see front matter © 2008 Elsevier Ltd. All rights reserved.
doi:10.1016/j.biomaterials.2008.12.010

the target cell population once localized to the tumor sites [9]. For targeted ^{10}B delivery in BNCT, immunoliposomes have been employed by linking tumor-targeting ligands to liposome such as antibodies or receptor ligands such as folate [10], transferrin [11] and epidermal growth factor (EGF) [12].

EGFR is a 170-kDa transmembrane tyrosine kinase and the *EGFR* gene is often amplified in human GBMs. EGFRvIII, which has an in-frame deletion of exons 2–7 of the extracellular domain of the *EGFR* gene, is constitutively expressed and amplified in up to 57% of GMBs [13,14]. EGFR is overexpressed in GMB, but is undetectable or weakly expressed in normal brain. Therefore, EGFR is an attractive molecular target for the specific delivery of therapeutic agents to high-grade gliomas [15,16]. An antibody can be directly linked to a liposome through covalent conjugation to a functional group on the liposome [17] or can be post-inserted into a preformed liposome via the micelles of an antibody–lipid conjugate [18,19].

We previously used hollow bionanocapsules (BNCs) composed of modified L protein (the hepatitis B virus surface antigen) for targeting brain tumors [20]. In the present study, BSH was encapsulated into a nickel-liposome and recombinant ZZ-His (IgG Fc-binding motif) was used as an adaptor to conjugate anti-EGFR antibody to the nickel-liposome, resulting in an immunoliposome. Three glioma cell lines, parental U87 glioma cells (PAU87) and human wild-type *EGFR* and *EGFRvIII*-transfected U87 glioma cells (U87 WT and U87 ΔEGFR), were used to evaluate the efficiency with which ^{10}B was delivered by the immunoliposomes *in vitro* and *in vivo*.

2. Materials and methods

2.1. Lipids and chemicals

1,2-Dioleoyl-*sn*-glycero-3-[(*N*-(5-amino-1-carboxypentyl)iminodiacetic acid)-succinyl] nickel (abbreviated as DOGS-NTA-Ni) and the fluorescent analog 25-[*N*-[(7-nitrobenz-2-oxa-1,3-diazol-4-yl)-methyl]amino]-27-norcholesterol (abbreviated as NBD-cholesterol) were purchased from Avanti Polar Lipids (Alabastar, AL). DOPC, DOPG and DSPE-PEG_{2000} were obtained from Nippon Oil and Fats (Tokyo, Japan). BSH ($Na_2B_{12}H_{11}SH$, ^{10}B enriched > 99%) was purchased from Katchem Ltd. (Czechoslovakia). Chloroform, diethyl ether and cholesterol were acquired from Wako Pure Chemicals (Japan).

2.2. Preparation of liposomes

Liposomes composed of DOPC:DOPG:DOGS-NTA-Ni:CH:DSPE-PEG_{2000} (3:3:1:4:0.1, molar ratio) were prepared according to the reverse-phase evaporation (REV) method [11] with slight modification. Briefly, 100 μmol of lipid was dissolved in 2 mL of a chloroform/diethyl ether mixture (1:1 v/v), and 1 mL of a 50 mM BSH solution was added. The ratio of the organic to aqueous phase was 2:1. To prepare liposomes for experiments *in vivo*, a 300 mM BSH solution was used. The mixture was sonicated for 1 min to form a W/O emulsion and evaporated with reduced pressure in a rotary evaporator at 50 °C until a gel was formed. Ten cycles of freezing (dry ice) and thawing (60 °C water bath) were then applied. To obtain liposomes with a homogeneous size distribution, the liposome emulsion was extruded through a polycarbonate membrane 100 nm in pore size using an extruder device at 60 °C. The mean diameter and zeta-potential of the prepared liposomes were determined with an electrophoretic light scattering spectrophotometer (ELS-8000, Photal, Tokyo, Japan). Unencapsulated free BSH was removed by an Amersham sephadex G-50 column (1 × 30 cm). For the preparation of fluorescent liposomes, 1 mol% of NBD-cholesterol was added to the lipid solution.

2.3. Expression and purification of ZZ-His protein

The ZZ gene was cloned into pET-22b (+) (Novagen, Madison, WI) and introduced into *E. coli* BL21 (DE3). The expression and purification of ZZ-His were performed as described [21]. Briefly, recombinant proteins were induced by the addition of 1 mM isopropyl-β-D-thiogalatopyranoside (IPTG) when the optical density (OD) of the cell culture at 600 nm reached 0.6. The expressed proteins were purified from the supernatant using ProBond Nickel-chelating resin (Invitrogen) and dialysed against PBS (pH 7.4) at 4 °C for 24 h. The proteins were stored at −80 °C prior to use.

2.4. Cell lines and cell culture

Three human glioma cell lines (kindly donated by Professor Webster K. Cavenee of the University of California at San Diego) were used. U87 ΔEGFR expresses EGFRvIII (145 kDa); U87 WT expresses wild-type EGFR (170 kDa); and PAU87 (parental) expresses no EGFR. The cells were maintained in Dulbecco's modified Eagle's medium (DMEM) (GIBCO) with 10% fetal bovine serum (FBS), penicillin and streptomycin at 37 °C in a humidified atmosphere containing 5% CO_2. Rat primary astrocytes were prepared from a newborn Wistar rat (Japan SLC, Inc.) as described previously [22].

2.5. Antibody-mediated ZZ delivery to EGFR-overexpressing glioma cells

To identify the ability of antibody-directed ZZ-His delivery, we first analyzed the expression level of EGFR in different cells. PAU87, U87 ΔEGFR, and U87 WT cells and primary astrocytes were homogenized by sonication in a boiling buffer containing 1% SDS and Western blotting was carried out as described previously [23]. The blots were probed with an anti-EGFR mouse mAb (101-7300-0, Katayama Chemical Inc., Japan) or the anti-EGFR rat mAb ICR10 (Abcam, Cambridge, UK). After incubation with the appropriate secondary antibody conjugated with horseradish peroxidase (Sigma–Aldrich), positive bands were visualized using an enhanced chemiluminescence detection system (Amersham Biosciences, Pittsburgh, PA).

For delivering ZZ-His into cells via antibody, 18 μg of ZZ-His and anti-EGFR mouse antibody were mixed at a molar ratio of 5 to 1 (ZZ-His to antibody) in 200 μL of PBS (pH 7.4) and rotated at 4 °C for 2 h. Then the ZZ-mAb complex was added to PAU87, U87 ΔEGFR, U87 WT and the primary astrocytes. As a control, only ZZ-His was added. After 2 h of incubation, the cells were washed with PBS twice and treated with 0.025% trypsin to remove surface-binding antibody. They were then resuspended in PBS twice before sonication and subjected to Western blotting using an anti-His (C-term) mouse monoclonal antibody (Invitrogen).

2.6. Analysis of liposome–ZZ–mAb complex (immunoliposome) by ultracentrifugation, Western blotting and lipid measurements

To determine the binding ability of nickel-liposomes and ZZ-His, the two were mixed at a molar ratio of 20–1 (nickel lipid: ZZ-His), rotated at room temperature for 1 h, and then subjected to sucrose gradient ultracentrifugation. Two milliliters of each 10, 20, 30, 40 and 50% sucrose solution was used to prepare the gradient. After 16 h of ultracentrifugation at 35,000 rpm using a Beckman coulter optima-LE-80k ultracentrifuge (rotor SW 41), 1 mL was drawn out and samples were resolved by SDS-PAGE and then transferred to nitrocellulose membranes (Hybond ECL, Amersham Biosciences). Western blotting was performed as described above. The lipid in each fraction was analyzed by the DAOS method using a Phospholipids C reagent kit (Wako Pure Chemical Inc. Ltd., Japan).

For a large amount of immunoliposome, the free ZZ protein was separated by a Sepharose CL-4B column (15 × 70 mm) and the collected liposome–ZZ was concentrated with Amicon Ultra-15 centrifugal filter devices (Millipore). The antibody was conjugated to the liposome–ZZ at a molar ratio of 1 to 20 (mAb:ZZ) and the free antibody was separated with a Sepharose CL-4B column.

2.7. Immunohistochemical analysis (IHC) and measurement of ^{10}B content in vitro

Immunoliposomes were prepared with anti-EGFR rat or mouse mAb for IHC and measuring ^{10}B content, respectively. IHC was carried out to analyze the distribution of ^{10}B *in vitro*. Cells were incubated for 24 h and BSH, liposome, liposome–ZZ, and immunoliposome were added. The final ^{10}B concentration was 1 μg/mL and the antibody concentration was 3 μg/mL. After 3 h of incubation, the cells were washed with PBS twice, fixed with 4% paraformaldehyde (PFA) for 10 min, and then incubated with anti-BSH mouse mAb [24]. The secondary antibody was Cy3-conjugated mouse IgG. Fluorescence signals were observed using a confocal laser microscope (FluoView, Olympus, Japan).

To detect ^{10}B in cells, BSH, liposome, liposome–ZZ, and liposome–ZZ–mAb were added in 6-cm dishes. After 3 h of incubation, the cells were washed with PBS, dissolved in 200 μL of concentrated nitric acid overnight, and diluted with 5 mL of MilliQ water. For liposome–ZZ and immunoliposome-treated cells, 250 mM of imidazole was used for an additional wash to remove surface-bound liposome. The ^{10}B content was measured by inductively coupled plasma-atomic emission spectrometry (ICP-AES, Vista Pro, Seiko Instruments, Japan).

To analyze the effect of the antibody concentration on the delivery of ^{10}B, 1 mM of liposome was incubated with U87 ΔEGFR cells in the presence of 0.1, 0.5, 1, 3, 5, 10, or 50 μg/mL of mAb for 3 h. To analyze the effect of time on the delivery, 3 μg/mL of antibody was used and U87 ΔEGFR cells were incubated with 1 mM of immunoliposome for 1, 3, 5, 7, 12 and 24 h. The ^{10}B measurements were carried out as described above.

2.8. Brain tumor model and detection of immunoliposomes in vivo

U87 ΔEGFR cells (5×10^5 cells/5 μL) were injected into the striatum of female 4- to-6 week-old nude mice (15-20 g, BALB/c Slc-nu/nu; Japan SLC) as described [24]. After two weeks, 400 μL of NBD-liposome and NBD-immunoliposome was administered into tumor-bearing mice intravenously via the tail. After 4 h and 24 h, the mice were sacrificed and the brains were placed in PBS. Sections of 10-μm thickness were cut on a microtome (CM 1850, Leica Microsystems, Wetzlar, Germany). IHC was

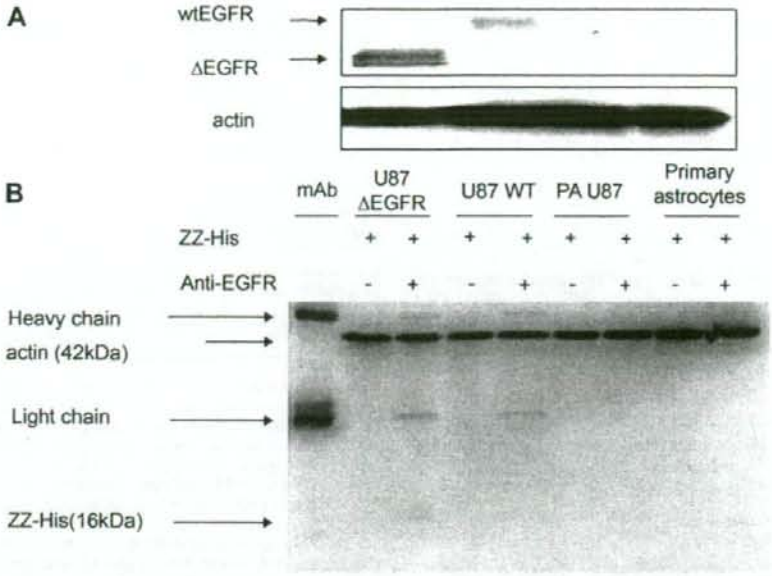

Fig. 1. EGFR expression level in different cell lines and antibody-mediated ZZ-His delivery. (A) Cell lysates of primary astrocytes and glioma cell lines U87 ΔEGFR, U87 WT, and PAU87 were subjected to 6% SDS-PAGE and transferred to PVDF membranes. Anti-EGFR mouse monoclonal antibody was used for detection of the wild-type and vIII EGFR. (B) ZZ-mAb and ZZ were incubated with cells for 2 h and the delivered proteins were detected by anti-His mouse mAb.

carried out as described above. The fluorescence labeling of liposomes was observed immediately after the sections were prepared.

For the analysis of the distribution of ^{10}B, immunoliposomes and liposomes were injected via the tail at a dose of 35 mg ^{10}B/kg. Tumor, normal brain, liver, and blood were sampled at 4, 12, 24, and 48 h post-administration, and the samples were digested with a nitric acid solution overnight and diluted with MilliQ water for ICP-AES.

2.9. Statistical analysis

Data are shown as the mean ± S.E. Data were analyzed using Student's *t*-test to compare the two conditions, and $p < 0.05$ was considered significant.

3. Results

3.1. Antibody-mediated delivery of ZZ into glioma cells

EGFR levels in each cell line were determined by Western blotting using an anti-EGFR monoclonal antibody (mAb). The mAb detected EGFR in ΔEGFR-expressing U87 cells (U87 ΔEGFR) and wild-type EGFR-expressing cells (U87 WT) (Fig. 1A). In contrast, EGFR expression was undetectable in PAU87 cells and primary astrocytes. Thereafter, we examined the ability of the mAb to target EGFR-overexpressing glioma cells. The Western blotting showed that the mAb and ZZ-His were detected in U87 ΔEGFR and U87 WT cells when ZZ was bound with the antibody (Fig. 1B). In contrast, neither mAb nor ZZ-His was detected without conjugation with the anti-EGFR mAb (Fig. 1B). Moreover, no antibody or ZZ was detected in PAU87 cells and primary astrocytes (Fig. 1B). These results suggest that the anti-EGFR mAb is capable of targeting glioma cells expressing wild-type and vIII EGFR.

3.2. Identification of liposome–ZZ–mAb complex

When 10 mol% of DOGS-NTA-Ni and 1 mol% of DSPE-PEG_{2000} were used in the liposome formulation, no aggregation occurred. It was reported that NTA-Ni increased the sensitivity and DSPE-PEG_{2000} reduced the aggregation [25]. Therefore, to identify the ability of ZZ-His to bind with mAb and nickel-liposomes containing 10 mol% DOGS-NTA-Ni and 1 mol% DSPE-PEG_{2000}, we carried out ultracentrifugation and Western blot analyses. The ultracentrifugation indicated that the nickel-liposomes bound with ZZ-His effectively. The positions in different layers are shown in Fig. 2A. When 1 mol% DSPE-PEG_{2000} was used in the liposome, the distribution was the same as that without DSPE-PEG_{2000} (data not shown). As shown in Fig. 2B, most of the PEG-liposomes were in the first layer after ultracentrifugation. When ZZ-His was mixed with the nickel-liposome and mAb, the liposomes occurred in the fourth and fifth layers. Results of Western blotting in Figs. 2C–F show that the ZZ, liposome, and antibody are all in the same layer (fractions 4 and 5), while free ZZ-His and mAb are in the first and third fractions, respectively. These results suggest that mAb is effectively bound to liposome via ZZ adaptor. When the molar ratio of nickel lipid to ZZ was 20:1, about half of the ZZ bound with liposomes (Fig. 2D). The ratio was adjusted to 40:1 in the subsequent experiment.

The Western blotting and lipid analysis also indicated that the binding of the nickel-liposome to ZZ and of ZZ to the mAb was specific because the liposome showed no ability to bind ZZ when nickel lipid was not used (data not shown). When ZZ was not used, the nickel-liposome showed no binding with mAb (data not shown). A scheme of the immunoliposome is shown in Fig. 3A. The diameter of the liposome is about 100 nm, but when ZZ and mAb are added, the diameter of the immunoliposome increases to 130 nm (Fig. 3B). The *z*-potential also increases, from −44.74 to −24.67 mV (Fig. 3C). The immunoliposomes were used for *in vivo* experiments.

3.3. Delivery of BSH into glioma cells in vitro

We examined the effect of the immunoliposomes on the delivery of ^{10}B in different cell lines. The cells were incubated with the immunoliposomes for 3 h and the delivery of ^{10}B was then investigated with IHC using the anti-BSH mAb (Fig. 4). BSH was not

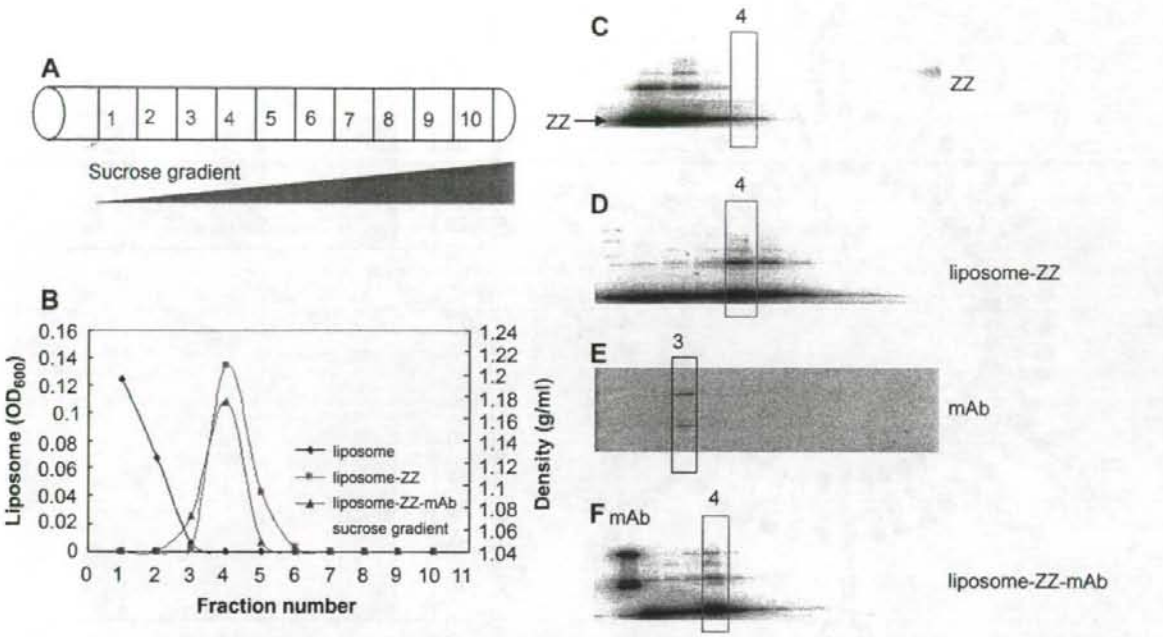

Fig. 2. Analysis of the liposome–ZZ–mAb complex. (A) Distribution of each fraction in a sucrose gradient. (B) Phospholipids in different fractions were measured by the DAOS method after ultracentrifugation and absorbance at OD_{600} was used to indicate the position of liposomes. (C, D) The position of ZZ was identified by anti-His antibody after ultracentrifugation in ZZ and liposome-ZZ samples. (E, F) The positions of mAb and ZZ were identified by anti-His antibody after ultracentrifugation in mAb and liposome–ZZ–mAb samples.

detected in primary astrocytes and only a small amount of BSH was delivered into PAU87 cells (Fig. 4). The results of ICP-AES were consistent with those of IHC (data not shown). In contrast, BSH was delivered in almost all U87 ΔEGFR and U87 WT cells expressing vIII EGFR and wild-type EGFR, respectively (Fig. 4). To demonstrate that BSH was actually present inside glioma cells and to exclude the possibility that it was just attached to the surface of the cells, serial optical sections of 2 μm taken along the *Z*-dimension of the immunostained cells were collected with a confocal microscope (Supplementary material). Signal for BSH on the surface of the cells was weak and most BSH was observed in the cells (Supplementary material). Moreover, strong signals were observed in the nucleus. To further investigate whether BSH delivered by immunoliposomes functions as ^{10}B in glioma cells, ICP-AES was performed (Fig. 5A). In U87 ΔEGFR and U87 WT cells incubated with control liposomes without the anti-EGFR antibody, the ^{10}B level was low. In contrast, a high level of ^{10}B was detected in the cells incubated with immunoliposomes (Fig. 5A). Moreover, immunoliposomes did not deliver ^{10}B into PAU87 cells (Fig. 5A). These results suggest that immunoliposomes conjugated with anti-EGFR antibodies efficiently deliver ^{10}B in glioma cells expressing EGFR.

3.4. Effect of antibody concentration and time course on BSH delivery

We examined the dose-dependent effect of the antibody on the efficiency of ^{10}B delivery. Following 3 h of incubation with immunoliposomes in the presence of 0.1, 0.5, 1, 3, 5, 10, or 50 μg/mL of anti-EGFR antibody, the cells were washed twice with PBS containing Ni-chelating components (250 mM imidazole) to remove surface-bound liposomes. ICP-AES revealed that 0.5 μg/mL of antibody was effective for the delivery of ^{10}B compared with liposomes without the antibody (Fig. 5B). In the time-course experiment, 3 μg/mL of antibody was used for the detection of ^{10}B and cells were incubated with immunoliposomes for 1, 3, 5, 7, 12 and 24 h. The ^{10}B content of cells increased with time (Fig. 5C). When cells were incubated with immunoliposomes at 4 °C, little ^{10}B was detected inside them (data not shown), suggesting that the uptake of immunoliposomes was temperature-dependent and the immunoliposomes were internalized into cells by endocytosis.

3.5. In vivo delivery of BSH in brain tumor by immunoliposomes

To observe the distribution of the liposome and BSH *in vivo*, we injected NBD-liposomes and NBD-immunoliposomes into the tail of nude mice two weeks at the tumor engraftment. In freshly prepared brain slices, fluorescence could be seen in the tumor and blood vessel wall 4 h after the injection (Figs. 6A and D). In normal tissues, strong fluorescence was seen only in the blood vessel wall (arrowheads in Fig. 6E). In the NBD-liposome-injected mice, no fluorescence was seen in the tumor (Fig. 6G). Signal's distribution indicates that the immunoliposomes were delivered into the tumor via the blood stream, and the delivery was antibody-dependent. BSH's distribution was examined by IHC using the anti-BSH mAb. BSH was clearly detected in the tumor whereas it was undetectable in normal tissue (Figs. 7A and B). A low level of BSH was observed in both tumor and normal tissues of the mice treated with the control liposome without conjugation of the anti-EGFR mAb (Figs. 7D and E). In immunoliposome-treated mice for 24 h, BSH was detected in the tumor and surrounding regions (Fig.7G and H).

We finally compared ^{10}B content among each tissue in this model of brain tumors. Immunoliposomes effectively delivered BSH to tumors compared with liposomes (Fig. 8). In immunoliposome-treated mice, the amount of ^{10}B in the tumor reached

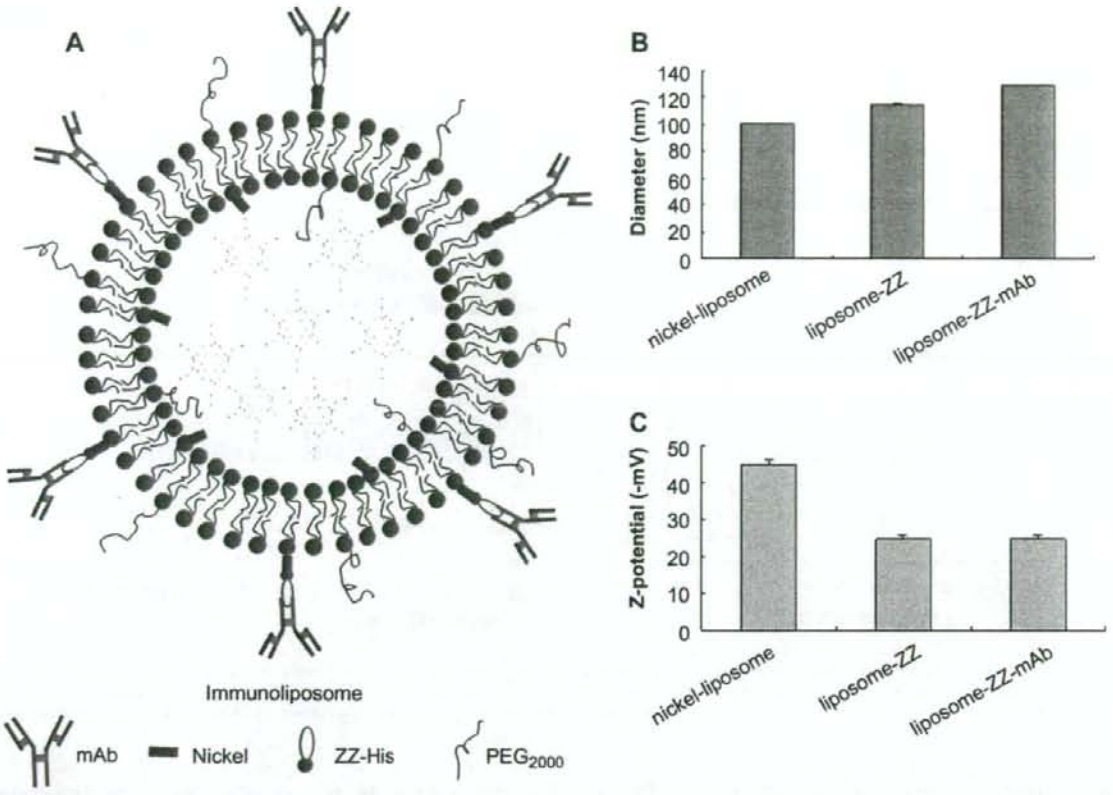

Fig. 3. Characteristics of the immunoliposomes. (A) Scheme of components of the immunoliposome. (B, C) Diameter and z-potential of the nickel-liposome, liposome–ZZ and immunoliposome.

28.36 ± 7.63 μg/g 24 h after the injection and remained high until the 48 h mark (21.38 ± 5.31 μg/g). In liposome-treated samples, on the other hand, the ^{10}B content of tumors at 24 and 48 h was 3.45 and 2.97 μg/g, respectively (Fig. 8A). In normal brain tissue of the mice treated with immunoliposomes and liposomes, ^{10}B content was low at all time points (Fig. 8B). In liver, ^{10}B levels peaked 12 h after the injection and then decreased in a time-dependent manner (Fig. 8C). In blood, ^{10}B levels reached a maximum 4 h after the injection of immunoliposomes and rapidly decreased 12 h after the injection (Fig. 8D).

4. Discussion

The aim of the present study was to develop a novel ^{10}B delivery system for targeting glioma cells. Since the appearance of BNCT in the 1950s, different methods of delivering ^{10}B into tumor cells have been investigated [2,4], though only BSH and BPA have been used clinically. BSH is thought to penetrate tumor tissue through a disrupted blood–brain barrier (BBB) and thus accumulates little in normal brain tissue [26]. BPA is an analog of an essential amino acid (tyrosine) and is actively taken up by tumor cells but also accumulates measurably in normal brain [5]. The specific accumulation of ^{10}B in tumor tissue is still a limitation to the use of this technology. In the present study, we encapsulated BSH in liposomes and used a universal adaptor (ZZ) to conjugate an anti-EGFR mAb to target glioma cells.

The wild-type EGFR and its isoforms (variant III) are considered prime targets for the specific delivery of a variety of diagnostic and therapeutic agents [9,27,28]. In BNCT, mAb or EGF-conjugated immunoliposomes and boronated mAb have been used to deliver ^{10}B into glioma cells [7,12,14,29]. The anti-EGFR antibody used in this study recognized both wild-type and vIII EGFR, so ZZ-His bound with the mAb could be effectively delivered into EGFR-overexpressing glioma cells. In our ^{10}B delivery system, the ability of ZZ to bind the nickel-liposome was not affected by the addition of 1% DSPE-PEG_{2000} and the liposome–ZZ complex showed the same position as the naked nickel-liposome–ZZ after ultracentrifugation (data not shown). Chikh et al. [30] reported that the addition of 5 mol% of DSPE-PEG_{2000} caused a slight change in the rate of binding, but the incorporation efficiency of His-tagged peptide did not change. The binding of DOGS-NTA-Ni with ZZ-His is not achieved at a theoretical ratio. When a molar ratio of 20:1 (DOGS-NTA-Ni:ZZ-His) was used, only about half the amount of ZZ could be conjugated with the liposome, and the liposome–ZZ complex was in the fourth layer (Fig. 2D). When the ratio was adjusted to 40:1, no free ZZ was detected by Western blotting after ultracentrifugation (data not shown). The interaction of DOGS-NTA-Ni with His-tags has been reported to be stronger than or equivalent to that of antibody interactions (10^{-6} to 10^{-9} M), with a dissociation constant (k_d) in the range of 10^{-6} to 10^{-13} M at pH 7–8 depending on the protein and location of the His-tag on the protein [31,32]. When the molar ratio of ZZ to mAb was 25:1, all the liposome–ZZ–mAb complexes occurred in the four and fifth layers after ultracentrifugation. For the preparation of immunoliposomes, removal of free ZZ and mAb from the liposome–ZZ complex may be important, because free mAb or ZZ–mAb will bind to EGFR-overexpressing cells.

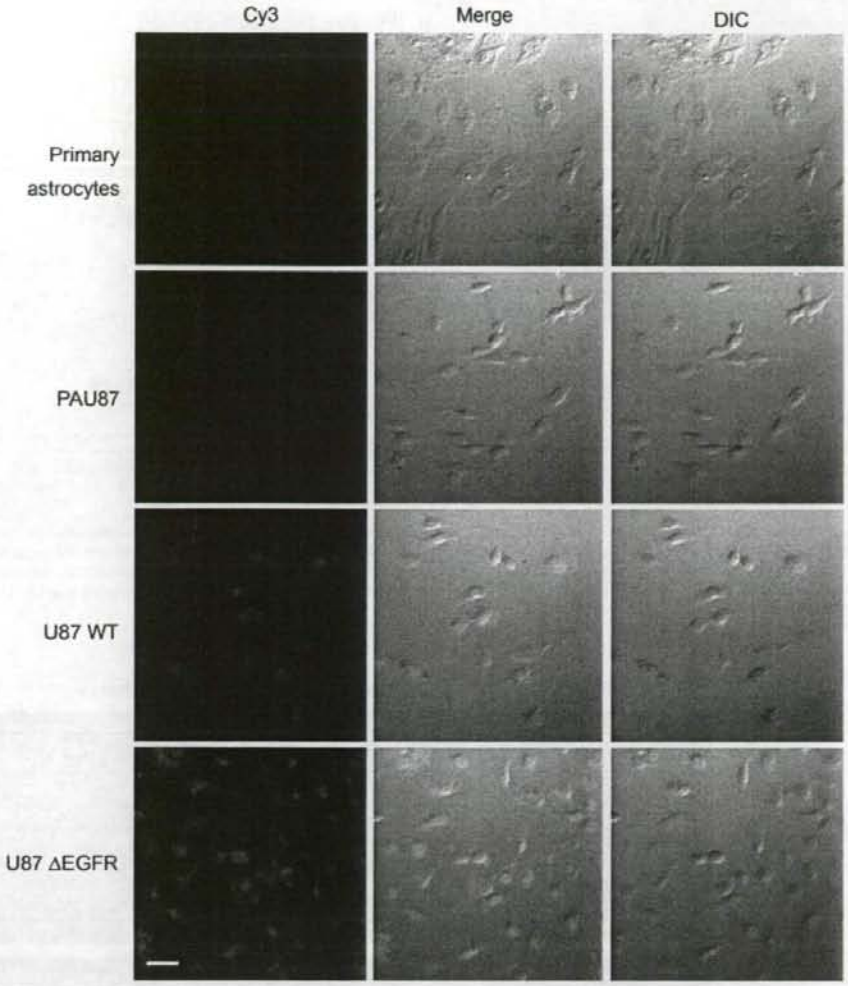

Fig. 4. Analysis by immunohistochemistry (IHC) of ^{10}B delivery by immunoliposomes in different cell lines. Immunoliposomes (liposome: 1 mM; anti-EGFR rat mAb: 3 μg/mL; ^{10}B: 1 μg/mL) were incubated with primary astrocytes, PAU87, U87 WT and U87 ΔEGFR for 3 h and fixed with 4% PFA. Anti-BSH mouse mAb was used as the primary antibody and Cy3-conjugated mouse IgG was used as the secondary antibody. The fluorescence signals were visualized using a confocal laser microscope. Bar = 50 μm.

The conjugation of ZZ-His protein at the surface of a liposome by DOGS-NTA-Ni will make the liposome more stable in blood. Moreover, the combination of ZZ and PEG inhibits interaction of the liposome and cells to some degree, and so inhibits non-specific endocytosis. Recently, NTA-Ni has been reported to attach His-tag peptides and proteins to the liposome [30]. van Broekhoven et al. [33] used NTA-Ni for surface mobilization of His-tagged antibodies for DC-specific receptor to DCs.

An advantage of using ZZ to bind with Fc of IgG is that complete-IgG-labeled liposomes may have shorter circulation times, due to the rapid identification and uptake of the Fc fragment by macrophages in circulation [34]. Allen et al. [35] reported that increasing the density of liposome-grafted antibodies resulted in a faster clearance of immnoliposomes from the circulation. To overcome this, an antibody fragment (Fab′ and scFV) that lacks the Fc portion was used, and showed identical circulation times with PEGylated non-immunolabeled liposome when conjugated to the free termini of PEGylated lipid [27].

Protein A has been widely used for purifying IgG because of its specific binding to the Fc domain of IgG through bioaffinity [36]. In this study, we used the ZZ motif (Fc-binding domain) as an adaptor to conjugate an antibody to the liposome, resulting in an immunoliposome. In this ^{10}B delivery system, the specificity and totality of the antibody are retained, and not affected by thiolation of the antibody during liposome's preparation. The His-tag at the C-terminus of ZZ is used not only for purification, but also for interaction with chelated divalent metal ions, nickel in the NTA-Ni lipid [37]. NTA forms a strong complex with four of the metal sites, leaving two additional sites for interaction with the His-tag present on the protein. After incubation in medium for 12 h, the immunoliposomes still deliver ^{10}B efficiently (data not shown), indicating the stability of liposome–ZZ–mAb in serum. Long-term stability of the immunoliposomes in serum will permit high levels of ^{10}B to accumulate in tumor cells *in vivo*.

Gliomas have a poor prognosis due to their exceptional ability to infiltrate normal brain tissue, often along blood vessels or nerve

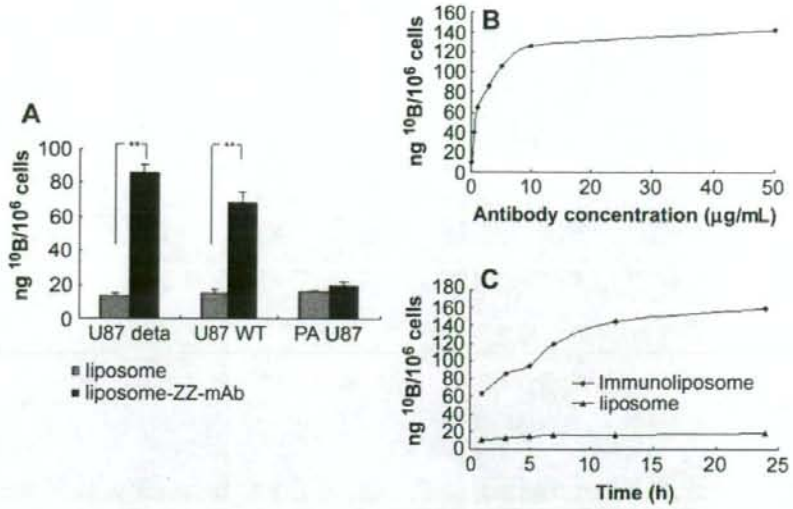

Fig. 5. ICP-AES of ^{10}B delivery by immunoliposomes *in vitro*. (A) After 3 h of incubation in medium containing 1 mM of liposomes or immunoliposomes (1 μg/mL of ^{10}B and 3 μg/mL of anti-EGFR mouse mAb) in a 6-cm dish, cells were treated with 0.025% trypsin and washed with 250 mM of imizadole and PBS, and amounts of internalized ^{10}B were detected. $n = 4$; ** $p < 0.01$. (B) Effect of antibody concentration on ^{10}B delivery. U87 ΔEGFR cells were incubated with 1 mM of immunoliposomes for 3 h in the presence of 0.1, 0.5, 1, 3, 5, 10, or 50 μg/mL of mAb and ^{10}B was detected. (C) Time course of ^{10}B delivery by immunoliposomes. Immunoliposomes and liposomes were incubated with U87 ΔEGFR cells for 1, 3, 5, 7, 12 and 24 h. At the indicated time, ^{10}B was measured.

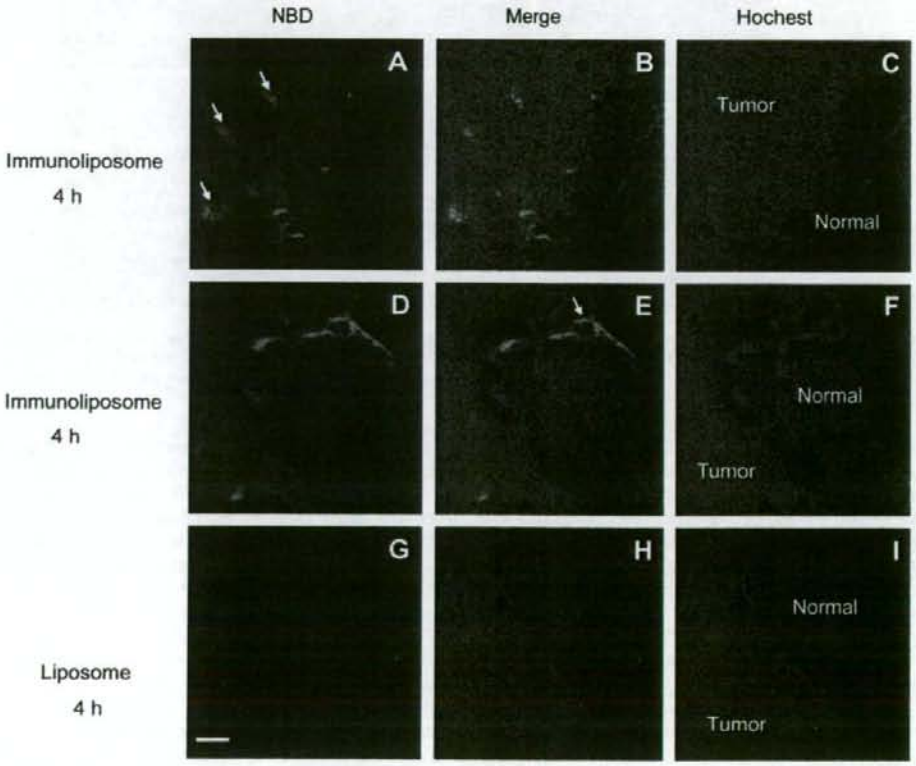

Fig. 6. Distribution *in vivo* of NBD-immunoliposomes. Four hundred microliters (liposome concentration: 50 mM; antibody concentration: 180 μg/mL) of NBD-immunoliposome or NBD-liposome was injected via the tail into nude mice two weeks after tumor engraftment. Green fluorescence of NBD and blue fluorescence of hochest were used to indicate the positions of the liposomes and tumor 4 h after injection, respectively. (A,D,G) NBD-fluorescence images (10×) of freshly prepared brain slices. (C,F,I) Hochest-fluorescence images (10×) of freshly prepared brain slices. (B,E,H) Merging of the NBD and hochest signals. Arrows indicate the positions of blood vessels. Bar = 200 μm.

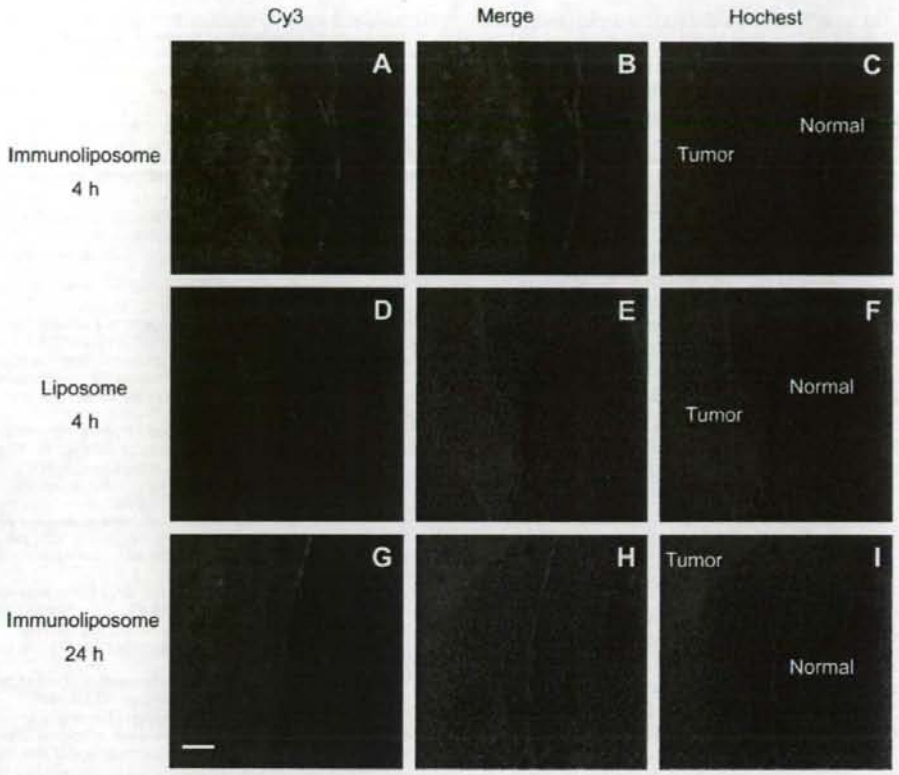

Fig. 7. IHC analysis of BSH's distribution *in vivo*. Four hundred microliters of immunoliposomes or liposomes was injected into the tail of nude mice two weeks after tumor engraftment. Slices were prepared 4 and 24 h post-injection. Anti-BSH mouse mAb and Cy3-conjugated mouse IgG were used as the primary and secondary antibody. Red fluorescence of Cy3 was used to show the distribution of BSH and blue fluorescence of hochest was used to indicate the position of the tumor. (A,D,G) Cy3-fluorescence images (10×). (C,F,I) Hochest-fluorescence images (10×). (B,E,H) Merging of the Cy3 and hochest signals. Bar = 200 μm.

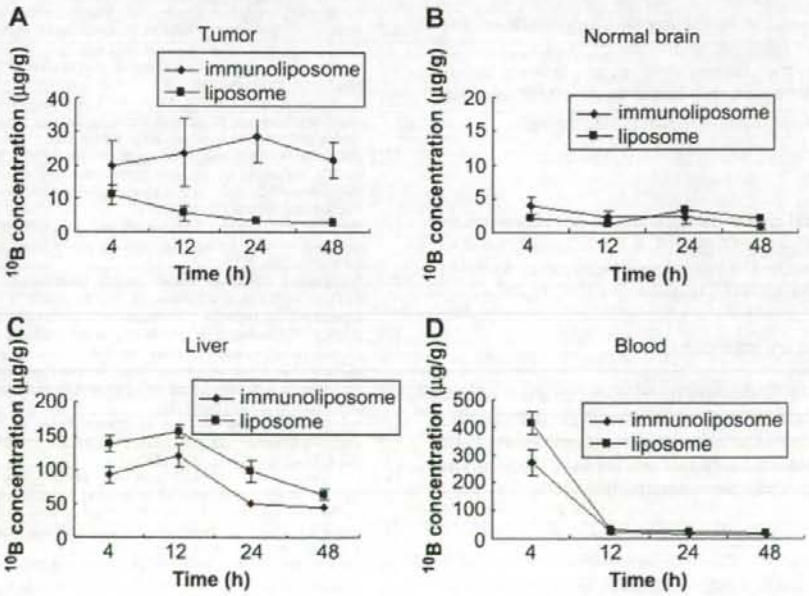

Fig. 8. Time course of ^{10}B's distribution *in vivo*. ^{10}B concentrations in tumor (A), normal brain (B), liver (C) and blood (D) were measured after 400 μL of immunoliposome or liposome was injected into tumor-bearing mice via a tail vein at a dose of 35 mg ^{10}B/kg.

fibers [38]. The tumor usually recurs after initial surgical resection. In BNCT, it is still difficult to deliver enough ^{10}B to the invading glioma cells in the brain. Our immunoliposomes may solve this problem. PEG-lipid and ZZ on the surface of the liposome provide steric stabilization and prolong circulation time. In solid tumors, the BBB is destroyed, and the abnormal tumor vessels are discontinuous, with pores varying from 100 to 780 nm [39,40]. At 4 h after an intravenous injection, the immunoliposome reached the tumor through the blood stream, and the anti-EGFR mAb effectively recognized the EGFR on the surface of tumor cells. The immunoliposomes had passed through the tumor vessel and penetrated tumor cells, as weak fluorescence could be seen in the blood vessel wall (Fig. 6A). At normal sites, we could see strong fluorescence on the surface of vessel walls and no fluorescence in normal tissues (Fig. 6E). This suggests that the immunoliposomes could not pass through the BBB in normal tissue.

To avoid possible toxic effects of DOGS-NTA-Ni, we are now exploring a new way to conjugate ZZ to the liposome surface. Our immunoliposomes can be used as a universal drug delivery system to deliver other anti-cancer drugs to tumor cells if we know the receptor or ligand on the surface of the tumor cells. In this study, ^{10}B delivery has been proved effective.

5. Conclusion

The results described above support the use of immunoliposomes to specifically deliver BSH to glioma cells. Recombinant ZZ-His (Fc-binding domain) was conjugated to liposomes containing 10 mol% DOGS-NTA-Ni and 1 mol% DSPE-PEG_{2000} to prepare immunoliposomes. This is the first time that an antibody-binding domain has been used to deliver ^{10}B in BNCT. ICP-AES and IHC indicated that ^{10}B was specifically delivered into EGFR-overexpresing glioma cells *in vitro* and *in vivo*. Thus, it appears that our system can be used for the specific delivery of other anti-cancer drugs.

Acknowledgements

We thank Dr. S. Kasaoka at Hiroshima International University for technical advice. This work was supported by a Grant-in-aid for Scientific Research from the Ministry of Education, Science, Sports and Culture of Japan and by a Grant-in-aid for Scientific Research from the Ministry of Health, Labour and Welfare of Japan.

Appendix

Figures with essential colour discrimination. Certain figures in this article, in particular parts of Figs. 2, 3, 4, 6 and 7, are difficult to interpret in black and white. The full colour images can be found in the online version, at doi:10.1016/j.biomaterials.2008.12.010.

Appendix. Supplementary material

Z-Dimensional scan of ^{10}B delivery by immunoliposomes in U87 ΔEGFR (100×). IHC was carried out as described in Fig. 4. Video was recorded at *Z*-sections from the bottom to top of cells every 2 μm. Supplementary data associated with this article can be found, in the online version, at doi:10.1016/j.biomaterials.2008.12.010.

References

[1] van Rij CM, Wilhelm AJ, Sauerwein WA, van Loenen AC. Boron neutron capture therapy for glioblastoma multiforme. Pharm World Sci 2005;27:92–5.
[2] Mehta SC, Lu DR. Targeted drug delivery for boron neutron capture therapy. Pharm Res 1996;13:344–51.
[3] Yanagië H, Ogata A, Sugiyama H, Eriguchi M, Takamoto S, Takahashi H. Application of drug delivery system to boron neutron capture therapy for cancer. Expert Opin Drug Deliv 2008;5:427–43.
[4] Barth RF, Coderre JA, Vicente MG, Blue TE. Boron neutron capture therapy of cancer: current status and future prospects. Clin Cancer Res 2005;11:3987–4002.
[5] Yokoyama K, Miyatake S, Kajimoto Y, Kawabata S, Doi A, Yoshida T, et al. Pharmacokinetic study of BSH and BPA in simultaneous use for BNCT. J Neurooncol 2006;78:227–32.
[6] Soloway AH, Hatanaka H, Davis MA. Penetration of brain and brain tumor. VII. Tumor-binding sulfhydryl boron compounds. J Med Chem 1967;10:714–7.
[7] Carlsson J, Kullberg EB, Capala J, Sjöberg S, Edwards K, Gedda L. Ligand liposomes and boron neutron capture therapy. J Neurooncol 2003;62:47–59.
[8] Hawthorne MF, Shelly K. Liposomes as drug vehicles for boron agents. J Neurooncol 1997;33:53–8.
[9] Sofou S, Sgouros G. Antibody-targeted liposomes in cancer therapy and imaging. Expert Opin Drug Deliv 2008;5:189–204.
[10] Pan XQ, Wang H, Lee RJ. Boron delivery to a murine lung carcinoma using folate receptor-targeted liposomes. Anticancer Res 2002;22:1629–33.
[11] Maruyama K, Ishida O, Kasaoka S, Takizawa T, Utoguchi N, Shinohara A, et al. Intracellular targeting of sodium mercaptoundecahydrododecaborate (BSH) to solid tumors by transferrin-PEG liposomes, for boron neutron-capture therapy (BNCT). J Control Release 2004;98:195–207.
[12] Bohl Kullberg E, Bergstrand N, Carlsson J, Edwards K, Johnsson M, Sjöberg S, et al. Development of EGF-conjugated liposomes for targeted delivery of boronated DNA binding agents. Bioconjug Chem 2002;13:737–43.
[13] Friedman HS, Bigner DD. Glioblastoma multiforme and the epidermal growth factor receptor. N Engl J Med 2005;353:1997–9.
[14] Yang W, Wu G, Barth RF, Swindall MR, Bandyopadhyaya AK, Tjarks W, et al. Molecular targeting and treatment of composite EGFR and EGFRvIII-positive gliomas using boronated monoclonal antibodies. Clin Cancer Res 2008;14:883–91.
[15] Schwechheimer K, Huang S, Cavenee WK. EGFR gene amplification-rearrangement in human glioblastomas. Int J Cancer 1995;62:145–8.
[16] Sauter G, Maeda T, Waldman FM, Davis RL, Feuerstein BG. Patterns of epidermal growth factor receptor amplification in malignant gliomas. Am J Pathol 1996;148:1047–53.
[17] Park JW, Hong K, Kirpotin DB, Papahadjopoulos D, Benz CC. Immunoliposomes for cancer treatment. Adv Pharmacol 1997;40:399–435.
[18] Ishida T, Iden DL, Allen TM. A combinatorial approach to producing sterically stabilized (Stealth) immunoliposomal drugs. FEBS Lett 1999;460:129–33.
[19] Iden DL, Allen TM. *In vitro* and *in vivo* comparison of immunoliposomes made by conventional coupling techniques with those made by a new post-insertion approach. Biochim Biophys Acta 2001;1513:207–16.
[20] Tsutsui Y, Tomizawa K, Nagita M, Michiue H, Nishiki T, Ohmori I, et al. Development of bionanocapsules targeting brain tumors. J Control Release 2007;122:159–64.
[21] Feng B, Zhao CH, Tanaka S, Imanaka H, Imamura K, Nakanishi K. TPR domain of Ser/Thr phosphatase of *Aspergillus oryzae* shows no auto-inhibitory effect on the dephosphorylation activity. Int J Biol Macromol 2007;41:281–5.
[22] Michiue H, Tomizawa K, Wei FY, Matsushita M, Lu YF, Ichikawa T, et al. The NH2 terminus of influenza virus hemagglutinin-2 subunit peptides enhances the antitumor potency of polyarginine-mediated p53 protein transduction. J Biol Chem 2005;280:8285–9.
[23] Tomizawa K, Iga N, Lu YF, Moriwaki A, Matsushita M, Li ST, et al. Oxytocin improves long-lasting spatial memory during motherhood through MAP kinase cascade. Nat Neurosci 2003;6:384–90.
[24] Doi A, Kawabata S, Iida K, Yokoyama K, Kajimoto Y, Kuroiwa T, et al. Tumor-specific targeting of sodium borocaptate (BSH) to malignant glioma by transferrin-PEG liposomes: a modality for boron neutron capture therapy. J Neurooncol 2008;87:287–94.
[25] Nielsen UB, Kirpotin DB, Pickering EM, Drummond DC, Marks JD. A novel assay for monitoring internalization of nanocarrier coupled antibodies. BMC Immunol 2006;7:24.
[26] Yokoyama K, Miyatake S, Kajiomoto Y, Kawabata S, Doi A, Yoshida T, et al. Analysis of boron distribution *in vivo* for BNCT using two different boron compounds by secondary ion mass spectroscopy. Radiat Res 2007;167:102–9.
[27] Mamot C, Drummond DC, Noble CO, Kallab V, Guo Z, Hong K, et al. Epidermal growth factor receptor-targeted immunoliposomes significantly enhance the efficacy of multiple anticancer drugs *in vivo*. Cancer Res 2005;24:11631–8.
[28] Mendelsohn J, Baselga J. Epidermal growth factor receptor targeting in cancer. Semin Oncol 2006;33:369–85.
[29] Pan X, Wu G, Yang W, Barth RF, Tjarks W, Lee RJ. Synthesis of cetuximab-immunoliposomes via a cholesterol-based membrane anchor for targeting of EGFR. Bioconjug Chem 2007;18:101–8.
[30] Chikh GG, Li WM, Schutze-Redelmeier MP, Meunier JC, Bally MB. Attaching histidine-tagged peptides and proteins to lipid-based carriers through use of metal-ion-chelating lipids. Biochim Biophys Acta 2002;1567:204–12.
[31] Lauer SA, Nolan JP. Development and characterization of Ni-NTA-bearing microspheres. Cytometry 2002;48:136–45.
[32] Patel JD, O'Carra R, Jones J, Woodward JG, Mumper RJ. Preparation and characterization of nickel nanoparticles for binding to His-tag proteins and antigens. Pharm Res 2007;24:343–52.
[33] van Broekhoven CL, Parish CR, Demangel C, Britton WJ, Altin JG. Targeting dendritic cells with antigen-containing liposomes: a highly effective

procedure for induction of antitumor immunity and for tumor immunotherapy. Cancer Res 2004;64:4357–65.
[34] Kamps JA, Scherphof GL. Receptor versus non-receptor mediated clearance of liposome. Adv Drug Deliv Rev 1998;32:81–97.
[35] Allen TM, Brandeis E, Hansen CB, Kao GY, Zalipsky S. A new strategy for attachment of antibodies to sterically stabilized liposome resulting in efficient targeting to cancer-cells. Biochim Biophys Acta 1995;1237:99–108.
[36] Moks T, Abrahmsén L, Nilsson B, Hellman U, Sjöquist J, Uhlén M. Staphylococcal protein A consists of five IgG-binding domains. Eur J Biochem 1986;156:637–43.
[37] Hochuli E, Döbeli H, Schacher A. New metal chelate adsorbent selective for proteins and peptides containing neighbouring histidine residues. J Chromatogr 1987;411:177–84.
[38] Laerum OD, Bjerkvig R, Steinsvåg SK, de Ridder L. Invasiveness of primary brain tumors. Cancer Metastasis Rev 1984;3:223–36.
[39] Maruyama K, Takahashi N, Tagawa T, Nagaike K, Iwatsuru M. Immunoliposomes bearing polyethyleneglycol-coupled Fab' fragment show prolonged circulation time and high extravasation into targeted solid tumors *in vivo*. FEBS Lett 1997;413:177–80.
[40] Siwak DR, Tari AM, Lopez-Berestein G. The potential of drug-carrying immunoliposomes as anticancer agents. Clin Cancer Res 2002;8:955–6.

Int. J. Oral Maxillofac. Surg. 2009; 38: 293–295
doi:10.1016/j.ijom.2008.12.010, available online at http://www.sciencedirect.com

International Journal of
Oral & Maxillofacial Surgery

Case Report
Head and Neck Oncology

Boron neutron capture therapy for papillary cystadenocarcinoma in the upper lip: A case report

Y. Kimura[1], Y. Ariyoshi[1], S. Miyatake[2], M. Shimahara[1], S. Kawabata[2], K. Ono[3]

[1]Department of Dentistry & Oral Surgery, Division of Medicine for Function & Morphology of Sensory Organs, Osaka Medical College, 2-7, Daigaku-machi, Takatsuki City, Osaka, Japan; [2]Department of Neurosurgery, Division of Surgery, Osaka Medical College, 2-7, Daigaku-machi, Takatsuki City, Osaka, Japan; [3]Particle Radiation Oncology Research Center, Research Reactor Institute, Kyoto University, 2-1010, Asashiro-nishi, Kumatori-cho, Sennan-gun, Osaka, Japan

Y. Kimura, Y. Ariyoshi, S. Miyatake, M. Shimahara, S. Kawabata, K. Ono: Boron neutron capture therapy for papillary cystadenocarcinoma in the upper lip: A case report. Int. J. Oral Maxillofac. Surg. 2009; 38: 293–295.

Abstract. Boron neutron capture therapy (BNCT) is a tumor-selective radiation therapy using α and ^{7}Li particles, which are produced by the reaction of neutron with boron (^{10}B), and taken up by the tumor. The authors report their first experience of BNCT on a patient with no history of surgery, chemotherapy or conventional radiotherapy for papillary cystadenocarcinoma in the upper lip.

Accepted for publication 9 December 2008

Boron neutron capture therapy (BNCT) is a tumor-selective radiation therapy that destroys cancer cells using α and ^{7}Li particles, which are generated by the reaction of thermal neutron with boron (^{10}B), and taken up by the tumor[4]. Clinical trials have studied the use of BNCT for brain tumors (cutaneous primary or cerebral metastasis from melanoma) and for head and neck cancer[3,7]. The authors have used BNCT to treat recurrent oral cancer and metastasis of lymph nodes after conventional treatment.

We report our first experience of using BNCT on a patient with no history of surgery (except biopsy), chemotherapy or conventional radiotherapy for papillary cystadenocarcinoma in the upper lip.

Case Report

An 78-year-old woman was referred with a 3-month history of mass formation in the upper lip. An extraoral examination revealed swelling in the left subnasal area. Intraorally, an irregularly shaped tumor mass was observed in the mucolabial fold from the upper left central incisor to the canine. The tumor mass was hard, with pitting ulceration on the surface, possibly due to contact with the edge of the upper denture. An incisional biopsy was performed, and papillary cystadenocarcinoma diagnosed. The patient refused surgical treatment, chemotherapy and radiotherapy. As a result, periodic follow-up was carried out on an outpatient basis.

The tumor gradually enlarged over three and a half years and surgery was recommended again; the patient refused. The possible course and prognosis, if observation was the only treatment, was explained to the patient. As a result, the patient consented to BNCT. The treatment was approved by the ethical committee of Osaka Medical College and by the BNCT committee of the Kyoto University Research Reactor Institute (KURRI).

At that time, the well-defined tumor was 40 × 30 × 25 mm in size, covering the area from the upper left lip mucosa to the buccal fold. Owing to pain and tenderness, the patient had difficulty using her dentures and eating. Magnetic resonance imaging (MRI) revealed a large space-occupying

0901-5027/030293 + 03 $30.00/0

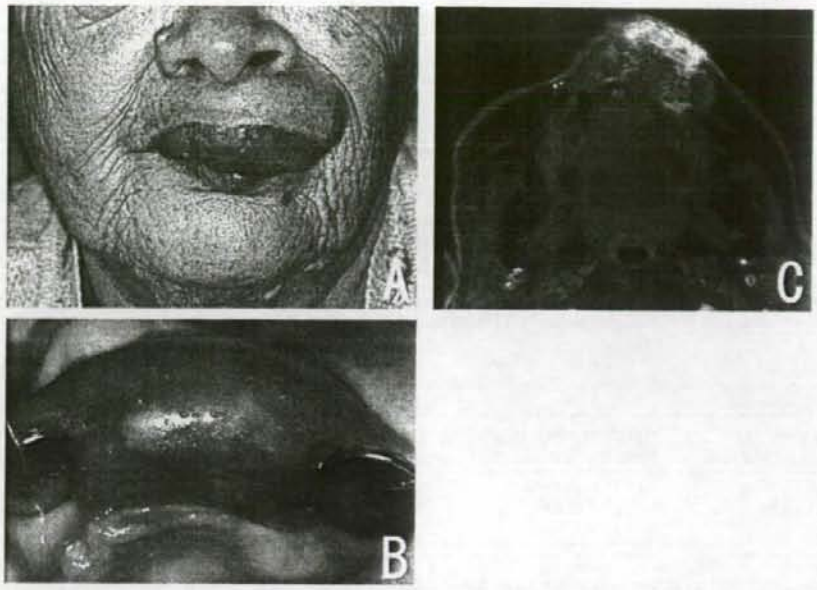

Fig. 1. (A, B) A large tumor mass that induced pain and difficulty in eating was seen in the left upper lip. (C) MRI (Gd-enhanced fat-suppressed image) revealed a large space-occupying mass lesion located in the left upper lip.

mass lesion located in the left upper lip (Fig. 1).

An ^{18}F-boronophenylalanine positron emission tomography (BPA-PET) examination[6] was performed on 15 December 2005 to investigate the uptake of BPA to the tumor. The ratio of boron uptake in the tumor to that in normal tissue (T/N ratio) was 3.2 (Fig. 2).

The first BNCT was performed under BPA (500 mg/kg) as an intravenous drip infusion at the KURRI[2,10] The authors applied the BNCT intentionally in 2 fractions at an interval of 4 weeks. The total dose was 63.4 Gy-Eq at the tumor peak and 59.8 Gy-Eq for the deepest portion (Table 1). Gy-Eq (Gy:Gray) is the biologically equivalent X-ray dose that would give an effect equivalent to that of total BNCT radiation.

The tumor tended to decrease in size after the first BNCT, and the second BNCT brought pain relief. An MRI after 5 months showed the tumor had shrunk by 86%. At present, 12 months after the second BNCT, the patient can wear full dentures, eat more easily and the pain has disappeared. MRI reveals shrinkage of the mass lesion (Fig. 3). Although mild stomatitis was observed after the first BNCT fraction, the patient was able to eat. Following the second fraction, extensive erosion developed in the oral mucosa associated with marked contact pain. After 2 weeks, the extensive erosion was cured. At the time of writing, the tumor has nearly disappeared macroscopically.

Fig. 2. Ratios of 18F-BPA accumulation in the area responsible for the tumor (upper lip) and normal tissues were assessed, and the T/N ratio was 3.2.

Discussion

A stable isotope of boron, ^{10}B divides to become an alpha and lithium particle when it captures a neutron. The sizes of those particles are about 9 μm and 4 μm, respectively, roughly equivalent to the size of cancer cells. In BNCT, ^{10}B is taken up by cancer cells where it reacts with neutrons during irradiation to destroy cancer cells selectively[3]. Farr et al.[5] were the first to use BNCT to treat a glioblastoma multiforme in 1954, since when the therapy has been carried out mainly for brain tumors. Mishima et al.[9] reported the results of using BNCT for a cutaneous malignant melanoma in 1989, and Kato et al.[7] reported using it for head and neck cancer in 2001. In the authors' hospital, BNCT

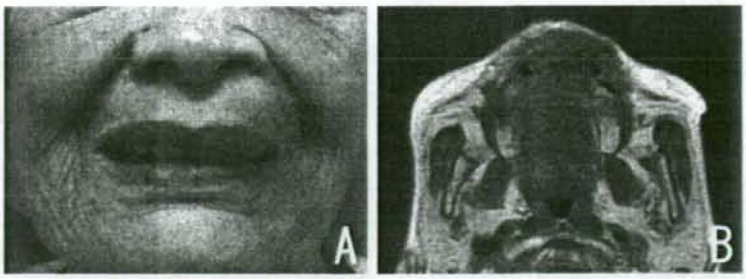

Fig. 3. (A) 12 months after treatment, the tumor mass had markedly decreased in size and the patient could wear full dentures and eat without difficulty. (B) There were no apparent high-signal areas on T2-weighted (fat-suppressed) images.

Table 1. BNCT parameters.

Dose (Gy-Eq)				
Fraction	Tumor peak (depth from skin surface, cm)	Minimum tumor (depth from skin surface, cm)	Oral mucosa	Irradiation time (min)
1	34.6 (2.5)	31.9 (3.5)	15.4	60
2	28.8 (2.5)	27.9 (3.5)	12.9	49
Total	63.4	59.8	28.3	109

has been used since 2005 for recurrent and/or advanced oral cancers that are difficult to treat using other therapies.

In general, malignant salivary gland tumors are considered to be radio-resistant, and radical surgery is the first treatment of choice[11]. BNCT is a tumor-selective, high LET radiation therapy with relatively high biological effect, therefore it should work well even for radio-insensitive tumors, compared with low LET radiation therapy using photons[8]. For head and neck cancer, KATO et al.[7] described the merits of BNCT as: the tissues and organs can be preserved; the therapy is effective for cases in which surgery is impossible; and it should be effective in squamous cell carcinoma, which is commonly involved in the head and neck, because the T/N ratio is high. AIHARA et al.[1] reported a case of recurrent mucoepidermoid carcinoma (high-grade malignancy) that responded well to BNCT. In the present case, as in the Aihara case, the T/N ratio in ^{18}F-BPA PET results had a relatively high value. The choice of this therapy should depend on the uptake of the boronic compound by the tumor not on the histologic type, including radiosensitivity, of the tumor.

The authors applied BNCT in 2 fractions at an interval of 4 weeks. The irradiation time for single-fraction BNCT would have been too long for the authors' elderly patient and the oral mucosa might have been damaged irreversibly by absorbing such a large dose.

One of the advantages of applying BNCT to head and neck tumors is its superficial location from the skin surface, making it possible to administer curative doses to the target using epithermal neutrons[7].

Acknowledgements. This work was supported in part by a Grant-in-Aid for Scientific Research (C) (No.18592224) to M. Shimahara from the Japan Society for the Promotion of Science and a grant from the Takeda Science Foundation to Osaka Medical College.

References

1. AIHARA T, HIRATSUKA J, MORITA N, UNO M, SAKURAI Y, MARUHASHI A, ONO K. Harada T: First clinical case of boron neutron capture therapy for head and neck malignancies using 18F-BPA PET. Head Neck 2006: **28**: 850–855.
2. ARIYOSHI Y, MIYATAKE S, KIMURA Y, SHIMAHARA T, KAWABATA S, NGATA K, SUZUKI M, MARUHASHI A, ONO K, SHIMAHARA M. Boron neutron capture therapy using epithermal neutrons for recurrent cancer in the oral cavity and cervical lymph node metastasis. Oncology Reports 2007: **18**: 861–866.
3. BARTH RF, CODERRE JA, VICENTE MG, BLUE TE. Boron Neutron Capture Therapy of Cancer: Current Status and Future Prospects. Clin Cancer Res 2005: **11**: 3987–4002.
4. CODERRE JA, MORRIS GM. Review: The Radiation Biology of Boron Neutron Capture Therapy. Radiation Res 1999: **151**: 1–18.
5. FARR LE, SWEET WH, ROBERTSON JS, FOSTER CG, LOCKSLEY HB, SUTHERLAND DL, MENDELSOHN ML, STICKLEY EE. Neutron Capture Therapy with Boron in the Treatment of Glioblastoma Multiforme. Am J Roentogenol Radium Ther Nucl Med 1954: **71**: 279–293.
6. IMAHORI Y, UEDA S, OHMORI Y, SAKAE K, KUSUKI T, KOBAYASHI T, TAKAGAKI M, ONO K, IDO T, FUJII R. Positron Emission Tomography-based Boron Neutron Capture Therapy Using Boronophenylalanine for High-Grade Gliomas: Part II. Clin Cancer Res 1998: **4**: 1833–1841.
7. KATO I, ONO K, SAKURAI Y, OHMAE M, MARUHASHI A, IMAHORI Y, KIRIHATA M, NAKAZAWA M, YURA Y. Effectiveness of BNCT for Recurrent Head and Neck Malignancies. Appl Radiat Isot 2004: **61**: 1069–1073.
8. KINASHI Y, MASUNAGA S, SUZUKI M, ONO K, OHNISHI T. Hyperthermia enhanced thermal neutron-induced cell death of human glioblastoma cell lines at low concentration of 10B. Int J Radiat Oncol Biol Phys 1998: **40**: 1185–1192.
9. MISHIMA Y, ICHIHASHI M, HATTA S, HONDA C, YAMAMURA K, NAKAGAWA T. New Thermal Neutron Capture Therapy for Malignant Melanoma. Melanogenesis-seeking 10B Molecular-Melanoma Cell Interaction from in vitro to First Clinical Trial. Pigment Cell Melanoma Res 1989: **2**: 226–234.
10. ONO K, MASUNAGA S, KINASHI Y, NAGATA K, SUZUKI M, SAKURAI Y, MARUHASHI A, KATO I, NAKAZAWA M, ARIYOSHI Y, KIMURA Y. Neutron irradiation under continuous BPA injection for solving the problem of heterogenous distribution of BPA. Advances in Neutron Capture Therapy 2006: 27–30.
11. SHINGAKI S, OHTAKE K, NOMURA T, NAKAJIMA T. The role of radiotherapy in the management of salivary gland carcinomas. J Craniomaxillofac Surg 1992: **20**: 220–224.

Address:
Yoshihiro Kimura
2-7 Daigaku-machi
Takatsuki City
Osaka 569-8686
Japan
Tel.: +81 72 683 1221
Fax: +81 72 681 3723.
E-mail: ora018@poh.osaka-med.ac.jp

J Neurooncol (2008) 89:239–246
DOI 10.1007/s11060-008-9621-6

CLINICAL-PATIENT STUDIES

Evaluation of fluoride-labeled boronophenylalanine-PET imaging for the study of radiation effects in patients with glioblastomas

Minoru Miyashita · Shin-Ichi Miyatake · Yoshio Imahori · Kunio Yokoyama · Shinji Kawabata · Yoshinaga Kajimoto · Masa-Aki Shibata · Yoshinori Otsuki · Mitsunori Kirihata · Koji Ono · Toshihiko Kuroiwa

Received: 14 April 2008 / Accepted: 28 May 2008 / Published online: 20 June 2008

Abstract Here we demonstrate that differentiation between glioblastoma (GB) tumor progression (TP) and radiation necrosis (RN) can be achieved with fluoride-labeled boronoalanine positron emission tomography (F-BPA-PET). F-BPA-PET images were obtained from histologically verified 38 GB, 8 complete RN, and 5 RN cases with partial residual tumors. The lesion/normal (L/N) ratios for these groups were 4.2 ± 1.4, 1.5 ± 0.3, and 2.0 ± 0.3, respectively. Ten GB patients underwent F-BPA-PET twice (once before and once after radiation treatment) due to enlargement of the original lesion or the development of new lesions post radiation. The L/N ratios of ten original site lesions had decreased by the second PET, and these lesions were revealed to be RN. In contrast, the L/N ratios of two lesions distant from the original site increased, and these lesions were revealed as cases of TP. Repeat PET imaging was found to be useful for evaluating changes in GB-associated tumor activity with respect to the treatment received.

Keywords Boronophenylalanine · Glioblastoma · Positron emission tomography · Radiation necrosis

M. Miyashita · S.-I. Miyatake (✉) · K. Yokoyama · S. Kawabata · Y. Kajimoto · T. Kuroiwa
Department of Neurosurgery, Osaka Medical College, 2-7 Daigaku-machi, Takatsuki, Osaka 569-8686, Japan
e-mail: neu070@poh.osaka-med.ac.jp

M.-A. Shibata · Y. Otsuki
Department of Anatomy & Cell Biology, Osaka Medical College, Takatsuki, Osaka, Japan

Y. Imahori
Cancer Intelligence Care System, Inc., Tokyo, Japan

M. Kirihata
Department of Agriculture, Osaka Prefectural University, Sakai, Osaka, Japan

K. Ono
Particle Radiation Oncology Research Center, Research Reactor Institute, Kyoto University, Kumatori, Osaka, Japan

Introduction

Glioblastoma (GB) is the most common primary malignant brain tumor. The treatment of patients with this pathology remains problematic. GB infiltrates into the normal brain parenchyma and is usually impossible to cure completely with surgical resection. Recently, new high-dose radiation therapies absorbed into the tumor tissue [e.g., boron neutron capture therapy (BNCT) and intensity-modulated radiotherapy (IMRT)] have been applied to treat patients with GB [1–4]. The efficacy of these treatments in eliciting clinical responses has been demonstrated in neuroimaging studies, in which lesions appear to have shrunk or the amount of peritumoral edema has decreased, and the associated clinical symptoms have likewise improved. Such radiation treatments and certain chemotherapeutic agents may alter the biological activity of tumor tissue, but it remains difficult to assess such changes.

It has been reported that high-dose, standard fractionated X-ray radiotherapy (XRT) has potential as a postoperative treatment for patients with supratentorial malignant gliomas [4]. Radiation necrosis (RN) was the most frequent adverse effect of radiation treatments, and excision of necrotic foci was required in some patients who had undergone standard XRT or IMRT [3, 4]. It remains important to evaluate the therapeutic effects of radiation therapy and chemotherapy on GB. Methods of treatment for RN and tumor progression (TP) differ substantially.

Radiotherapy and chemotherapy combined with salvage surgery must be considered for TP, and RN may be treated initially, primarily using medical approaches (steroids, anticoagulants, vitamin E, etc.) [5–12]. Necrotic tissue should be excised when medical treatment means fail to control an increase in perifocal edema around a lesion. However, from a clinical perspective, it remains difficult to differentiate between these pathological conditions using ordinary neuroimaging technologies such as magnetic resonance imaging (MRI) and computed tomography (CT).

Here we examine and describe how to evaluate the biological activity of GB and how to differentiate radiation necrosis from GB tumor progression using positron emission tomography (PET) with fluoride-labeled boronophenylalanine (F-BPA) as a tracer.

Materials and methods

Patients

Thirty-eight patients with GB underwent an F-BPA-PET study. All patients were treated at the Department of Neurosurgery, Osaka Medical College, from January 2002 to December 2006, and received follow-up care until December 2007. Among these 38 patients, 19 had recurrent disease (those who had previously been treated with surgery and radiation treatments), and 19 were newly diagnosed with GB. All patients underwent surgery after being included in the study and the pathology results confirmed GB as the correct diagnosis after the patients underwent F-BPA-PET. In 10 of these 38 patients, F-BPA-PET was performed twice, i.e., once before treatment, including surgical resection followed by radiotherapy, and primarily with BNCT (this was defined as the first PET study); and once again after treatment, when enhanced lesions were enlarged at the original site (OS) or had newly appeared distant from the OS, as shown by follow-up gadolinium (Gd)-enhanced MRI. We defined the latter PET study as the second PET. We also categorized ten patients who underwent F-BPA-PET twice as belonging to a "twice-PET" group. In this latter group, following the second F-BPA-PET, seven patients received surgical resection of new or reappearing and enlarged lesions, and histological diagnoses were confirmed as RN or TP. The other lesions in the twice-PET group were followed monthly with Gd-MRI. If the lesions grew during the follow-up period, we considered them to constitute TP, and if they remained stable in size and shape, or decreased in size during the follow-up period (>4 months), we considered them to be RN. The profiles of the patients in this group are given in Table 1. Six lesions in four other patients, including patients with GB and other malignancies such as metastatic brain tumors, were also given F-BPA-PET once only, when it was suspected that their intracranial lesions were RN, the sequelae of radiation therapy. All six lesions were histologically diagnosed as being either RN or RN in the main portion, with some residual tumor cells. We categorized these six lesions in these four patients as belonging to the "once-PET" group (Table 2).

PET scan

All F-BPA-PET scans were performed at Nishijin Hospital, Kyoto, Japan. BPA was originally synthesized as described previously [13, 14] and the protocol for the PET measurements using a HEADTOME III (Shimadzu Co., Kyoto, Japan) has also been described elsewhere [15, 16]. Briefly, regional BPA incorporation into tumors and contralateral brain tissue (as a nontumorous control area) was measured on PET images after an intravenous injection of F-BPA at a dose of 37–55.5 MBq (1–1.5 mCi) per 10 kg of body weight. PET images were collected continuously for a 60-min period, for a total of 15 periods. The lesions on the PET images were confirmed using contrast-enhanced MRI performed at levels equivalent to those used for the PET imaging studies. To obtain quantitative measurements using Amide software (SourceForge, Inc.), oval regions of interest (ROIs) were placed on the tumors, including peak values in tumors of various sizes. At the corresponding level, the contralateral brain area was also chosen for ROI analysis. All of the macroscopically necrotic tumor areas observed on MRI were excluded when the ROIs were designated. We designated several ROIs from tumor-affected areas, and adopted regions with the highest values as representative ROIs. We determined each ROI at least 1 cm^2 at real area size.

Statistical analysis

The L/N ratios of the 38 cases were analyzed using the Mann-Whitney U test, and the data from the first and second PET in the twice PET group were analyzed with the Wilcoxon matched-pair signed-rank test using StatView version 5.0 (SAS Institute, Inc.). We considered p values of less than 0.05 as statistically significant.

Results

The L/N ratios of histologically verified GB cases and RN cases

We applied F-BPA-PET to examine 38 cases of histologically verified GB. The L/N ratio of these 38 cases was 4.2 ± 1.4 (mean ± standard deviation [SD]). We first compared

Table 1 Patient characteristics who undergone F-BPA-PET two times (twice-PET group)

	Pre-Tx	L/N at first F-BPA-PET	Additional Tx	L/N at second F-BPA-PET	Result
Case 1		3.5	BNCT, XRT	1.9	RN (histological)
Case 2		2.6	BNCT, XRT	1.8	RN (clinical)
Case 3	XRT	3.3	BNCT	1.6	RN (histological)
Case 4		4.8	BNCT, XRT	1.8	RN (clinical)
Case 5		2.1	BNCT, XRT	1.4	RN with viable tumor cells (histological)
Case 6	SRS	5.0	BNCT, XRT	0.9	RN (histological)
Case 7 (OS)		4.3	BNCT, XRT × 2	1.9	RN (histological)
(RL)				3.1	TP (clinical)
Case 8 (OS)	XRT	2.6	BNCT	1.7	RN (clinical)
(RL)				2.9	TP (clinical)
Case 9	XRT	4.0	BNCT	2.1	RN with viable tumor cells (histological)
Case 10	XRT	3.7	BNCT	2.2	RN with viable tumor cells (histological)

BNCT: boron neutron capture therapy
Clinical: speculation by clinical course
Histological: histologically confirmed
OP: operation
OS: original site
RL: remote lesion
RN: radiation necrosis
SRS, SRT: stereotactic radiosurgery, or therapy
TP: tumor progression
Tx: treatment
XRT: X-ray radiation therapy

Table 2 Patient characteristics, histologically verified RN (once-PET group)

Case	Pretreatment diagnosis	Treatment	L/N at F-BPA-PET after Tx	Histological diagnosis
Case 11	Meta	SRS × 2	1.4	Complete RN
Case 12	Meta	SRS × 2	2.2	RN with viable tumor cells
Case 13	GB	SRS, XRT	1.7	Complete RN
Case 14	GB	XRT	2.1	RN with viable tumor cells
Case 15	None*	XRT, BNCT × 2	1.5	Complete RN
Case 16	None*	XRT, BNCT × 2	1.4	Complete RN

None: No enhanced lesion was observed at intracranial before BNCT was performed for adenoductal carcinoma of parotid gland. Case 15 and 16 is the identical case but different lesions at frontla and temporal, respectively

the L/N ratios of newly diagnosed GB with those of recurrent GB cases. The L/N ratios of newly diagnosed GB were 2.1 to 7.1 (4.3 ± 1.3) and those of recurrent GB cases were 2.6 to 7.0 (3.9 ± 1.4). There was no significant difference between the L/N ratios these two groups ($p = 0.16$), as shown in Fig. 1a. Next, we compared the L/N ratios of these histologically verified GB cases to those of histologically verified RN cases. The latter were composed of eight complete RN cases (four from the twice-PET group and four from the once-PET group), and five cases of primarily RN with partial residual tumor tissue (three from the twice-PET group and two from the once-PET group). The L/N ratios were 1.5 ± 0.3 and 2.0 ± 0.3, respectively. There were marked differences in the L/N ratios between GB cases (both the newly diagnosed and recurrent cases) and RN cases (both the complete necrosis cases and cases of necrosis in the main region, with partial residual tumor tissue, verified histologically) ($p < 0.01$), as shown in Fig. 1b. There was a statistically significant difference in L/N ratios between necrosis cases and cases of necrosis in the main region, with partial residual tumor tissue, in all histologically verified cases ($p = 0.03$) (Fig. 1a).

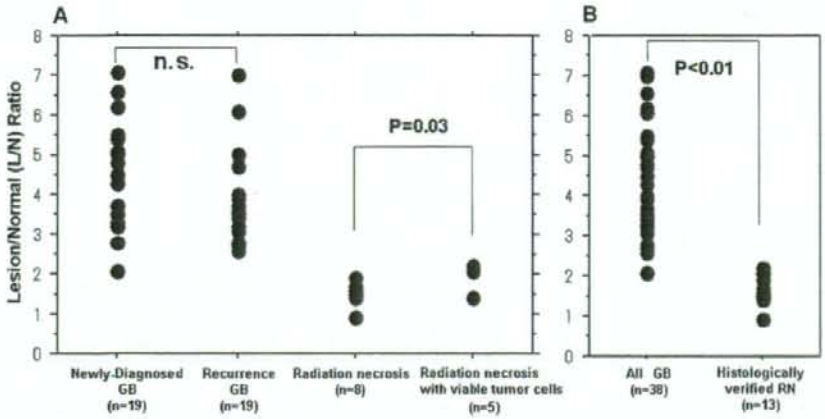

Fig. 1 (**a**) The L/N ratios in histologically verified newly diagnosed and recurrent GB cases and in histologically verified RN cases with and without tumor components. The L/N ratios of newly diagnosed GB cases ranged from 2.1 to 7.1 (4.3 ± 1.3), and those of recurrent cases ranged from 2.6 to 7.0 (3.9 ± 1.4). There was no significant difference in the L/N ratio between newly diagnosed and recurrent GB cases ($p = 0.16$). Histologically verified RN cases were composed of eight complete RN cases (four from the twice-PET group and four from the once-PET group), and five primarily RN cases with partial residual tumors (one from the twice-PET group and two from the once-PET group). There was a significant difference in the L/N ratio for complete RN cases and primarily RN cases with partial residual tumors ($p = 0.03$). (**b**) The L/N ratios in all GB cases and in histologically verified RN cases with and without tumor components. Significant statistical differences were observed in both groups ($p < 0.01$)

The L/N ratios of first versus second BPA-PET studies

In the twice PET group, we compared the L/N ratios between the first and the second PET studies. In all ten cases, BPA accumulation at OS in the second PET scan was lower than that in the first PET scan (Table 1 and Fig. 2). The L/N ratios in the first PET scan were 2.1 to 5.0 (3.5 ± 0.9). There was no significant difference between the L/N ratio of the first PET and that of all 38 cases ($p = 0.34$). In the second PET, the L/N ratio of the ten lesions at OS was 0.9 to 2.2 (1.7 ± 0.3). There was a significant difference between the L/N ratios of the ten lesions at OS in the second PET scan and those in the first PET scan ($p < 0.01$), as shown in Fig. 2. All ten lesions at OS were judged as RN. Seven of these lesions were histologically verified as RN, and the remaining three were considered to be RN based on the clinical course. Moreover, the L/N ratios of the lesions judged as RN were statistically different from those of cases of total GB and also from those of cases of recurrent GB ($p < 0.01$). There was no significant difference between the L/N ratio of histological RN cases ($n = 13$ in Tables 1 and 2) and that of cases of clinical RN ($n = 3$ in Table 1) ($p = 0.89$).

On the other hand, the L/N ratios in the second PET study obtained from the two lesions distant from the OS were 2.9 and 3.1 (cases 7 and 8 in Table 1, and open triangles in Fig. 2). These lesions were not verified as TP by histological examination, whereas the clinical courses of both lesions suggested a high possibility of TP, because follow-up MRI showed rapid growth of both lesions,

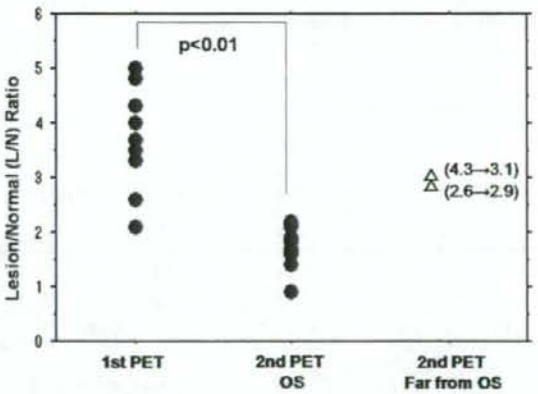

Fig. 2 Comparison of the L/N ratios in the GB of the first PET with that of the second PET. Filled circles and open triangles express the L/N ratios at the original site and remote lesions, respectively. Filled circles on the second PET were all cases of RN (seven cases histologically verified, and three cases clinically suspected). Open triangles indicate the non-OS L/N ratio and that for lesions clinically considered as TP. Statistical significance was observed in the L/M ratios between the first PET and the second PET at OS ($p < 0.01$)

whereas the lesions at OS of the same cases were stable in size and judged as RN.

Illustrative cases

Case 6: GB treated with surgical resection and BNCT (Table 1 and Fig. 3)

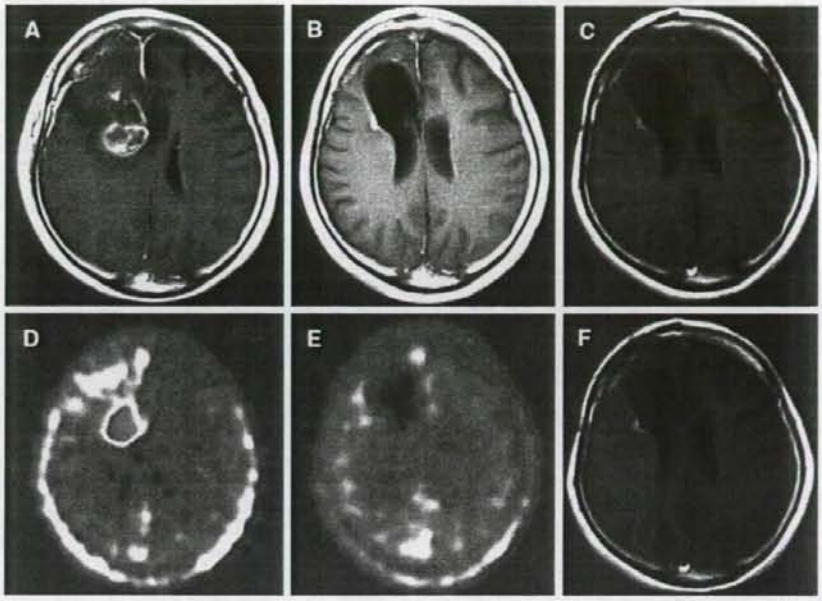

Fig. 3 A representative case (case 6): GB treated by surgical resection and BNCT. Glioblastoma treated by surgical resection followed by BNCT and 40 Gy conventional XRT. (**a**) Gd-MRI taken just prior to the second surgery. (**b**, **c**) Periodic follow-up MRI. (**d**) First PET, taken just prior to the second surgery, showing high F-BPA accumulation; L/N 5.0. (**e**) Second PET, taken 6 months after BNCT. The L/N ratio was 0.9 in this PET, suggesting radiation necrosis of the enhancement-positive lesion. (**f**) No enlargement of this enhanced lesion was recognized in follow-up MRI for 10 months after the last surgery

This is a patient with a glioma in the right frontal lobe. Surgical resection was applied, and the histological diagnosis was anaplastic oligodendroglioma. After the operation, adjuvant therapy was administered (chemotherapy with nimustin, procarbazin, and vincristin and stereotactic radiosurgery (SRS) for the enhanced lesion). Eight months after the final chemotherapy treatment, local recurrence was observed on MRI. The patient was referred to our clinic, and the first PET suggested tumor recurrence (L/N ratio 5.0, Fig. 3a, d). The second surgical resection was performed, and the histological diagnosis of the surgical specimen was GB with oligodendroglioma component. After the second operation, BNCT was performed, with a minimum tumor dose of 37.3 Gy-Eq: (Gray-equivalent), i.e., a biologically equivalent X-ray dose that can yield effects equivalent to total particle radiation with BNCT; also in addition, the maximum normal tissue dose of 8.34 Gy-Eq and conformal XRT was added to treat the deep lesion (40 Gy). Six months after the second operation, a locally enhanced lesion with perifocal edema was recognized on MRI, and the patient underwent a second PET. The L/N ratio was 0.9 in the second PET study, suggesting RN of the enhanced lesion (Fig. 3b, e). No enlargement of the enhanced lesion was obtained in the follow-up Gd-enhanced MRI at 10 months, and a clinical diagnosis of radiation necrosis was given (Fig. 3c, f). The patient wanted histological confirmation that the lesion was truly RN, and therefore we performed a surgical biopsy. The histological diagnosis was pure necrosis; no tumor cells were found.

Case 7: GB recurrence treated with surgical resection, BNCT, and XRT twice (Table 1 and Fig. 4)

This is a patient with glioblastoma in the right parietal lobe. The first surgical resection was performed and the histological diagnosis was GB. Before first resection, MRI and F-BPA-PET were carried out (Fig. 4a, b). The L/N ratio of the OS in the first PET study was 4.3. After gross total resection, BNCT was performed with a minimum tumor dose of 50.5 Gy-Eq, and a maximum normal tissue dose of 13.3 Gy-Eq, and for a deep lesion, XRT (30 Gy) was added. Ten months after BNCT, a new lesion appeared at the bottom of the cavity where the previous lesion had been removed, and this lesion had invaded to the splenium at the opposite side. Additional 50 Gy XRT was applied with two opposed right–left beams, followed by chemotherapy with Temozolomide; this approach controlled growth of the lesion for another 8 months. After this period of stabilization, the enhanced lesion at the OS was enlarged and some enhanced lesions far from the OS were detected in follow-up MRI (Fig. 4c, d). The patient exhibited left hemiparesis due to perifocal edema of the enhanced lesion at the OS. A second surgical resection was performed on the OS lesion to control the perifocal edema. Prior to the second operation, a second PET study was carried out (Fig. 4e, f). The L/N ratio of the lesion at the OS was 1.9. On the other hand, the L/N ratio of the remote enhanced lesion was 3.1, and we arrived at a diagnosis of TP due to cerebrospinal fluid dissemination. The surgical specimen from the second operation showed radiation necrosis (Fig. 4g). The OS lesion was not enlarged on follow-up MRI, but the remote lesion rapidly enlarged.

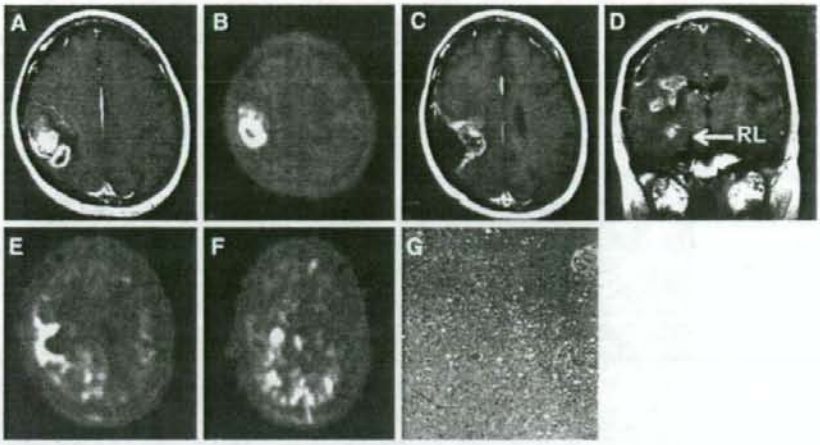

Fig. 4 A representative case (case 7): GB treated with surgical resection, BNCT, and XRT × 2. (**a**, **b**) Initial Gd-MRI and F-BPA-PET (First PET) just prior to the first surgery; the L/N ratio was 4.3. (**c**, **d**) Follow-up MRI 1.5 years after BNCT and XRT × 2 prior to the second surgery. The enhanced lesion of OS lesion was enlarged, and a remote lesion (RL), which was considered to have disseminated, was observed. (**e**, **f**) Second PET was performed, and the L/N ratio of the OS lesion was 1.9, which suggested radiation necrosis of the enhancement-positive lesion; the L/N ratio of the RL was 3.1, which on this PET study was suggestive of tumor progression. (**g**) A second surgical specimen was confirmed histologically to be RN

Discussion

New modalities for the treatment of malignant gliomas (MG), and primarily of GB, have recently been introduced. In addition, new chemotherapeutic agents such as Temozolomide are being developed for the treatment of MG [17]. The main approach to the adjuvant treatment of MG remains radiotherapy, and this approach is also advancing. To date, not only conventional XRT and SRS, but also new brachytherapies such as gliasite [18] and IMRT, a particle radiation modality, have been developed to administer highly absorbed doses to tumorous tissue with high conformity [1, 3, 19]. In addition, BNCT, a tumor-selective targeting particle radiation treatment, has been used for the treatment of malignant brain tumors [2, 20, 21]. These new modalities are steadily improving the results of MG treatment, although local high-dose radiation itself increases the possibility of RN. Even BNCT, if applied in recurrent cases, carries the risk of RN due to previous XRT exposure, as shown in Table 1.

It is important to differentiate between RN and TP when determining the optimal radiation dose for high-dose radiation studies such as BNCT, IMRT, and particle radiation therapies. If we consider a lesion to be TP, the radiation dose should be increased, whereas if it is deemed to be a case of RN, the radiation dose should be decreased at the next step of a radiation study. It is crucial to distinguish correctly between RN and TP, because the appropriate treatment differs for each pathological condition after diagnosis. If an incorrect diagnosis leads to the application of the wrong treatment, the treatment itself may decrease the patients' quality of life or even shorten survival. In many cases, earlier diagnosis may also lead to a better outcome.

A number of modalities for differentiating between RN and malignant tumor recurrence have been studied, including thallium-single photon emission computed tomography (SPECT) [22] and magnetic resonance spectroscopy (MRS) [23]. Among such approaches, PET imaging has undergone rigorous scrutiny as it allows for the direct analysis of tissue metabolism. In some patients with suspected RN who underwent F-BPA-PET and surgery, we applied MRS mapping. Moreover, in some of our cases, MRS and PET yielded the same results (RN), while in other cases, no lactate and lipid peaks, which are indicators of RN on MRS, correctly, while F-BPA-PET suggested RN, and histological examination confirmed the diagnosis of RN (data not shown).

In addition, a number of different tracers have been used for PET imaging to detect malignant tumors. Fluorodeoxyglucose (FDG) has been used and studied in numerous tumor types [24]. The brain shows high sugar metabolism, and FDG-PET reveals a very high metabolic background in the normal brain. Moreover, FDG accumulates well in cases of inflammation [25]. However, inflammatory cells commonly infiltrate at the RN border as well as in normal brain tissue [21, 26]. Therefore, it remains rather difficult to apply FDG-PET for discriminating between RN and TP [27]. It has been reported that, in some RN cases, FDG accumulates well in the absence of evidence of tumor

recurrence [28]. PET imaging using amino acids as tracers is promising for the detection of malignant tumors in the brain, because the background activity of protein metabolism in the brain is rather low in comparison with that of sugar. ^{11}C-labeled methionine (MET) has been used as a tracer for amino-PET [29, 30]. This tracer has been used for analyzing metabolism in malignant brain tumors [29, 30] as well as for differentiating between RN and TP [30]. A known potential disadvantage of ^{11}C-labeled substances such as methionine is that, due to the short half-life of the tracer, they are unavailable to PET centers without a cyclotron [31]. On the other hand, ^{18}F-labeled substances have a longer half-life. We confirmed that the addition of boron to phenylalanine at the phenyl radical improves biodistribution over that achieved with naïve phenylalanine. Phenylalanine itself tends to become trapped at the liver if it is administered systemically. We speculate that the addition of boron at the phenyl radical in phenylalanine inhibits the nonspecific uptake of the tracer in the lever in comparison with that of naïve phenylalanine [32, 33]. Originally we and others undertook F-BPA-PET studies for the purpose of BNCT [32–34]. One of the present authors (Y.I.) reported that the accumulation of this tracer correlates well with clinical malignancy and correlates inversely with patient survival [15, 16, 32, 33]. In addition, the accumulation of this tracer may enable differentiation between RN and TP, as described here. Here, a marked difference between the L/N ratios of GB and RN was observed; the lowest L/N ratio in GB listed here was 2.1, and the highest L/N ratio was 2.2, in cases primarily consisting of RN with a partial tumor residue. Therefore, it remains difficult to distinguish between RN and TP in all cases, especially when only a single F-BPA-PET evaluation is performed.

Finally, it should be kept in mind that, even in patients with L/N ratios of <2.0, viable or recurrent tumor cells may be present in the tissue. We identified some tumor cells in the majority of necrotic tissues when necrotic tissue was removed, even in patients with L/N ratios of less than 2.0, as shown in Table 1. The majority of tissues can only be deemed necrotic if the L/N ratio is below 2.0. In such cases, the RN must be removed and/or treated with various therapies such as steroids, anticoagulants, hyperbaric oxygenation, and vitamin E.

Conclusions

There were significant differences between GB tumor progression and radiation necrosis in the L/N ratios observed on F-BPA-PET imaging. An L/N ratio on F-BPA-PET of greater than 2.5 is strongly suggestive of TP, and an L/N ratio of less than 2.0 suggests a high possibility of RN.

Acknowledgments This work was partly supported by a Grant-in-Aid for Scientific Research (B) (16390422, 19390385) from the Japanese Ministry of Education, Culture, Sports, Science, and Technology to Shin-Ichi Miyatake. This work was also supported in part by the Takeda Science Foundation for Osaka Medical College. We are also grateful to Mr. Horii at Nishijin Hospital for technical support with the PET study.

References

1. Narayana A, Yamada J, Berry S, Shah P, Hunt M, Gutin PH, Leibel SA (2006) Intensity-modulated radiotherapy in high-grade gliomas; clinical and dosimetric results. Int J Radiat Oncol Biol Phys 64:892–897
2. Miyatake S, Kawabata S, Kajimoto Y, Aoki A, Yokoyama K, Yamada M, Kuroiwa T, Tsuji M, Imahori Y, Kirihata M, Sakurai Y, Masunaga S, Nagata K, Maruhashi A, Ono K (2005) Modified boron neutron capture therapy for malignant gliomas performed using epithermal neutron and two boron compounds with different accumulation mechanisms: an efficacy study based on findings on neuroimages. J Neurosurg 103:1000–1009
3. Iuchi T, Hatano K, Narita Y, Kodama T, Yamaki T, Osato K (2006) Hypofractionated high-dose irradiation for the treatment of malignant astrocytomas using simultaneous integrated boost technique by IMRT. Int J Radiat Oncol Biol Phys 64:1317–1324
4. Tanaka M, Ino Y, Nakagawa K, Tago M, Todo T (2005) High-dose conformal radiotherapy for supratentorial malignant glioma: a historical comparison. Lancet Oncol 6:953–960
5. Burger P, Boyko O (1991) The pathology of central nervous system radiation injury. In: Gutin PH, Leibel SA, Sheline GE (eds) Radiation injury to the nervous system. Raven Press, New York, pp 191–208
6. Delanian S, Balla-Mekias S, Lefaix JL (1999) Striking regression of chronic radiotherapy damage in a clinical trial of combined pentoxifylline and tocopherol. J Clin Oncol 17:3283–3290
7. DiLorenzo N, Nolletti A, Palma L (1978) Late cerebral radionecrosis. Surg Neurol 10:281–290
8. Eyster EF, Nielsen SL, Sheline GE, Wilson CB (1974) Cerebral radiation necrosis simulating a brain tumor. Case report. J Neurosurg 40:267–271
9. Glantz MJ, Burger PC, Friedman AH, Radtke RA, Massey EW, Schold SC Jr (1994) Treatment of radiation-induced nervous system injury with heparin and warfarin. Neurology 44:2020–2027
10. Kusske JA, Williams JP, Garcia JH, Pribram HW (1976) Radiation necrosis of the brain following radiotherapy of extracerebral neoplasms. Surg Neurol 6:15–20
11. Martins AN, Johnston JS, Henry JM, Stoffel TJ, Di Chiro G (1977) Delayed radiation necrosis of the brain. J Neurosurg 47:336–345
12. Rizzoli HV, Pagnanelli DM (1984) Treatment of delayed radiation necrosis of the brain. A clinical observation. J Neurosurg 60:589–594
13. Ishiwata K, Ido T, Mejia AA, Ichihashi M, Mishima Y (1991) Synthesis and radiation dosimetry of 4-borono-2-[18F]fluoro-D L-phenylalanine: a target compound for PET and boron neutron capture therapy. Int J Rad Appl Instrum [A] 42:325–328
14. Mishima Y, Imahori Y, Honda C, Hiratsuka J, Ueda S, Ido T (1997) In vivo diagnosis of human malignant melanoma with positron emission tomography using specific melanoma-seeking 18F-DOPA analogue. J Neurooncol 33:163–169
15. Imahori Y, Ueda S, Ohmori Y, Kusuki T, Ono K, Fujii R, Ido T (1998) Fluorine-18-labeled fluoroboronophenylalanine PET in patients with glioma. J Nucl Med 39:325–333